

Combined high-resolution seismostratigraphic and morphobathymetric analysis reveals glacial history of the northwestern Chukchi margin, Arctic Ocean

Sookwan Kim¹, Leonid Polyak², Young Jin Joe¹, Frank Niessen³, Hyoung Jun Kim¹, Yeonjin Choi¹, Seung-Goo Kang¹, Jong Kuk Hong¹, Seung-II Nam¹, and Young Keun Jin¹

¹Korea Polar Research Institute

²Ohio State University

³Alfred Wegener Institute Helmholtz Centre for Polar and Marine Research

November 26, 2022

Abstract

High-resolution seafloor mapping provides insights into the dynamics of past ice-sheets/ice-shelves on high-latitude continental margins. Geological/geophysical studies in the Arctic Ocean suggest widespread Pleistocene ice grounding on the Chukchi–East Siberian continental margin. However, flow directions, timing, and behavior of these ice masses are not yet clear due to insufficient data. We present a combined seismostratigraphic and morphobathymetric analysis of the Chukchi Rise off the northwestern Chukchi margin using the densely acquired sub-bottom profiler (SBP) and multibeam echosounder (MBES) data. Comparison with deeper airgun seismic records shows that the SBP data cover most of the glaciogenic stratigraphy possibly spanning ca. 0.5–1 Ma. Based on the stratigraphic distribution and geometry of acoustically transparent glaciogenic diamictos, the lateral and vertical extent of southern-sourced grounded ice became smaller over time. The older deposits are abundant as debris lobes on the slope contributing to a large trough mouth fan, whereas younger till wedges are found at shallower depths. MBES data show two sets of mega-scale lineations indicating at least two fast ice-streaming events of different ages. Contour-parallel recessional morainic ridges mark a stepwise retreat of the grounded ice margin, likely controlled by rising sea levels during deglaciation(s). The different inferred directions of ice advances and retreats reflect complex geomorphic settings on the borderland. The overall picture shows that the Chukchi Rise was an area of intense interaction(s) of different ice-sheets/ice-shelves. In addition to glaciogenic deposits, we identify a number of related or preceding seabed features including mounds, gullies/channels, and sediment waves.

1 **Combined high-resolution seismostratigraphic and morphobathymetric analysis**
2 **reveals glacial history of the northwestern Chukchi margin, Arctic Ocean**

3 **Sookwan Kim^{1*}, Leonid Polyak², Young Jin Joe^{1,3}, Frank Niessen⁴, Hyoung Jun Kim¹,**
4 **Yeonjin Choi^{1,5}, Seung-Goo Kang¹, Jong Kuk Hong¹, Seung-II Nam¹, and Young Keun**
5 **Jin^{1*}**

6 ¹Korea Polar Research Institute, Incheon, 21990, Republic of Korea

7 ²Byrd Polar and Climate Research Center, The Ohio State University, 1090 Carmack Road,
8 Columbus, OH, 43210, USA

9 ³Department of Earth and Marine Sciences, Jeju National University, Jeju, 63243, Republic of
10 Korea

11 ⁴Alfred Wegener Institute (AWI), Helmholtz Centre for Polar and Marine Research, D-27568,
12 Bremerhaven, Germany

13 ⁵Korea Maritime and Ocean University, Busan, 49112, Republic of Korea

14 *Corresponding authors: S. Kim (skwan@kopri.re.kr) and Y. K. Jin (ykjin@kopri.re.kr)

15
16 **Key Points:**

- 17 • Detailed sub-bottom profiler and multibeam echosounder data were acquired at the
18 northwestern Chukchi margin.
- 19 • The new geophysical data grid reveals a three-dimensional geometry and distribution of
20 glaciogenic sediments and geomorphic features.
- 21 • Seafloor mapping results indicate four major glacial events with variable grounded ice
22 extent and flow direction.
23

24 **Abstract**

25 High-resolution seafloor mapping provides insights into the dynamics of past ice-sheets/ice-
26 shelves on high-latitude continental margins. Geological/geophysical studies in the Arctic Ocean
27 suggest widespread Pleistocene ice grounding on the Chukchi–East Siberian continental margin.
28 However, flow directions, timing, and behavior of these ice masses are not yet clear due to
29 insufficient data. We present a combined seismostratigraphic and morphobathymetric analysis of
30 the Chukchi Rise off the northwestern Chukchi margin using the densely acquired sub-bottom
31 profiler (SBP) and multibeam echosounder (MBES) data. Comparison with deeper airgun
32 seismic records shows that the SBP data cover most of the glaciogenic stratigraphy possibly
33 spanning ca. 0.5–1 Ma. Based on the stratigraphic distribution and geometry of acoustically
34 transparent glaciogenic diamictons, the lateral and vertical extent of southern-sourced grounded
35 ice became smaller over time. The older deposits are abundant as debris lobes on the slope
36 contributing to a large trough mouth fan, whereas younger till wedges are found at shallower
37 depths. MBES data show two sets of mega-scale lineations indicating at least two fast ice-
38 streaming events of different ages. Contour-parallel recessional morainic ridges mark a stepwise
39 retreat of the grounded ice margin, likely controlled by rising sea levels during deglaciation(s).
40 The different inferred directions of ice advances and retreats reflect complex geomorphic settings
41 on the borderland. The overall picture shows that the Chukchi Rise was an area of intense
42 interaction(s) of different ice-sheets/ice-shelves. In addition to glaciogenic deposits, we identify
43 a number of related or preceding seabed features including mounds, gullies/channels, and
44 sediment waves.

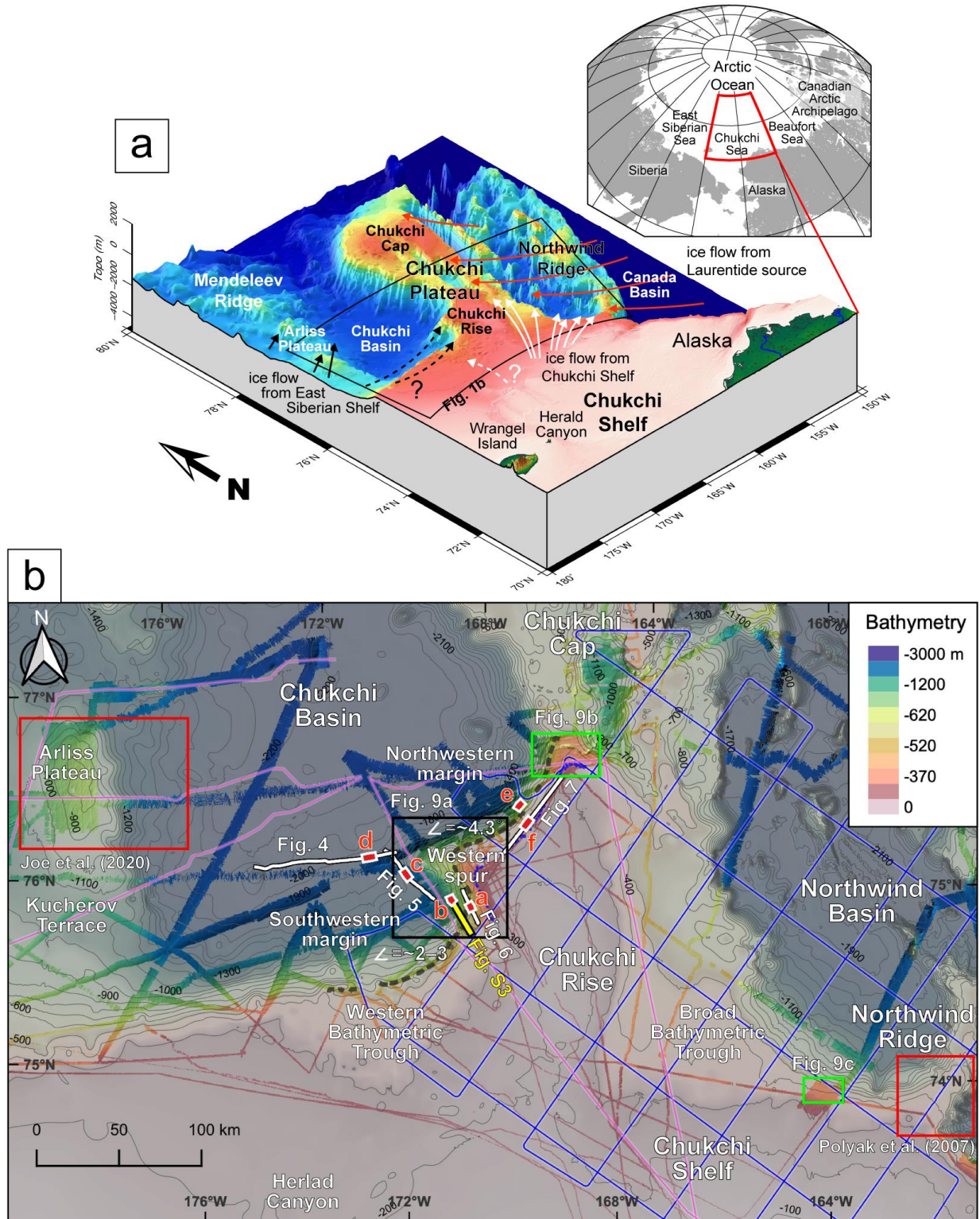
45

46 **1 Introduction**

47 Understanding the dynamics of marine-based ice sheets is a critical prerequisite for
48 predicting the responses of modern glacial systems to the warming climate and rising sea levels
49 (e.g., DeConto & Pollard, 2016; Howat et al., 2007). This task requires thorough geological and
50 geophysical investigation of high-latitude continental margins and adjacent borderlands for
51 understanding the build-up and decay mechanisms of the past ice sheets (Dowdeswell et al.,
52 2016 and references therein). While comprehensive data have been collected from the Polar
53 North Atlantic margins since the late 20th century (Elverhøi et al., 1998), the Quaternary glacial
54 history of the Arctic Ocean remained largely speculative until the last two decades. Recent
55 marine geophysical data employing high-resolution seafloor mapping technologies indicate the
56 extensive impact of grounded ice-sheets/ice-shelves on the continental margins, as well as
57 bathymetric highs in the central Arctic Ocean (Dove et al., 2014; Jakobsson, 1999; Jakobsson et
58 al., 2008, 2014, 2016; Niessen et al., 2013; Polyak et al., 2001). In particular, a wealth of new
59 data has been collected from the Chukchi–East Siberian margin and the adjacent borderland in
60 the western Arctic Ocean since the late 2000s due to the rapid retreat of sea-ice cover (Coakley
61 et al., 2011; Darby et al., 2005; Jokat, 2009; SWERUS Scientific Party, 2016). The acquired data
62 demonstrate a complex pattern of grounded-ice impact on the seafloor interpreted as recurring
63 glacial flows from the Laurentide, East Siberian, and Chukchi ice centers (Dove et al., 2014;
64 Jakobsson et al., 2005, 2008, 2014; Niessen et al., 2013; Polyak et al., 2007). This picture
65 indicates a critical role of this region for understanding the overall Arctic glacial history, while
66 the timing, extent, and provenance of glacial events remain poorly known.

67 In this paper, we focus on the western side of the Chukchi Rise, a geological structure
68 extending north from the Chukchi continental shelf (Figure 1). The Chukchi Rise and adjacent
69 seafloor structures were shown to have multiple glaciogenic bedforms indicative of glacial flows
70 potentially originating from the Laurentide, East Siberian, and Chukchi ice-spreading centers
71 (Dove et al., 2014; Jakobsson et al., 2008, 2014; Polyak et al., 2001, 2007) (Figure 1a). The
72 western Chukchi Rise facing the East Siberian margin is a key but poorly constrained area for
73 understanding these glacial interactions. We analyze new, detailed seismostratigraphic and
74 geomorphic data from this area for empirical constraints on past ice-sheet dynamics and related
75 sedimentary processes. Our analysis is based on the combined high-resolution sub-bottom
76 profiler (SBP) and multibeam echosounder (MBES) data revealing previously unexplored
77 sedimentary structures, stratigraphy, and submarine landforms. These densely collected
78 geophysical data (Figure 1b) allow for tracing the three-dimensional geometry of individual
79 seafloor and subsurface formations, which provide clues for spatio-temporal distribution of the
80 depositional/erosional glaciogenic features and related seabed forming processes (Dowdeswell et
81 al., 2004, 2016; C. H. Eyles & Eyles, 2010; Rebesco et al., 2016). This empirical evidence
82 augments sediment-core stratigraphy from neighboring areas (Joe et al., 2020; Polyak et al.,
83 2007; Schreck et al., 2018) and ice sheet modeling studies (Colleoni et al., 2016; Gasson et al.,
84 2018), and thus sheds new light on the glacial history of the Chukchi–East Siberian continental
85 margin. The generated data also provide valuable context for potential scientific drilling projects
86 in the western Arctic Ocean.

87



88

89 **Figure 1.** (a) Location map of the Chukchi Borderland in the Arctic Ocean (upper right inset)
 90 and a bathymetric map of the Chukchi Borderland (IBCAO version 4.0; Jakobsson et al., 2020).
 91 Color-coded arrows indicate ice flow directions inferred in prior studies (Dove et al., 2014;

92 Jakobsson et al., 2008, 2014; Niessen et al., 2013; Polyak et al., 2001); from the East Siberian
 93 (black), Chukchi margin (white), and Laurentide source (red); dashed arrows indicate more
 94 tentative interpretations. A black fan-shaped rectangle outlines the study area shown in panel 1b.
 95 **(b)** Data location map of the western side of the Chukchi Rise subdivided into the northwestern
 96 and southwestern margins and the western spur. Multibeam bathymetry data collected by the
 97 IBRV *Araon* (bright-colored) is overlaid on the regional bathymetry (dim-colored) with 100-m
 98 contour intervals. Thick white lines are the key SBP data shown in Figures 4 to 7. Labeled thick
 99 red segments are locations of the SBP data columns *a–f* in Figure 2. The black rectangle outlines
 100 the detailed survey area shown in Figures 9a and S5. Other rectangles show the location of
 101 additional ARA03B data (green, Figures 9b and 9c) and the study areas from Polyak et al. (2007)
 102 on the Northwind Ridge and Joe et al. (2020) on the Arliss Plateau (red). White numbers show
 103 the upper slope gradients. Blue and purple lines are regional geophysical data grids of MGL1112
 104 (Coakley et al., 2011; Dove et al., 2014) and ARK-XXIII/3 (Hegewald & Jokat, 2013; Jokat,
 105 2009), respectively. A thick yellow line crossing the outer shelf to the upper-mid slope is a
 106 multichannel seismic profile along the trough mouth fan at the southwestern margin (Figure S3).
 107 Dark gray and blue dashed lines are 600-mwd and 350-mwd isolines marking the shelf edge and
 108 the limit of iceberg plowmarks, respectively.

109

110

111 **2 Background**

112 The Chukchi Borderland in the western Arctic Ocean is comprised of the north–south
 113 trending bathymetric highs and troughs (Hall, 1990) (Figure 1a). The Chukchi Rise is an
 114 immediate extension of the Chukchi Shelf separated by a saddle-like depression from the
 115 Chukchi Cap to the north (Hegewald & Jokat, 2013; Shaver & Hunkins, 1964). The Chukchi
 116 Basin to the west and the Northwind Basin to the east separate the Chukchi Rise from the East
 117 Siberian margin and the Northwind Ridge, respectively. The relatively flat top shelf of the
 118 Chukchi Rise has ~200 m water depth (mwd) and less than 0.1° of slope gradient measured along
 119 a ~100 km north-south transect (Jakobsson et al., 2020). The western side of the Chukchi Rise
 120 shelf has a generally steeper inclination (ca. $0.5\text{--}0.7^\circ$) from the crest to the shelf break at ~500–
 121 600 mwd than the eastern side (ca. 0.3°). The slope gradient from the shelf break to middle slope
 122 at ~1000–1100 mwd varies from gentler (ca. $2.6\text{--}3.3^\circ$) in the southwestern Chukchi Rise to
 123 steeper (ca. 4.6°) in the northwestern Chukchi Rise (white numbers in Figure 1b). The mid-lower
 124 slope gradient (from ~1100 to 2200 mwd) on the southwestern margin is $\sim 0.6^\circ$. A triangular-
 125 shaped bathymetric high, named the western spur in this study, protrudes westward from the
 126 middle of the Chukchi Rise ~20 km into the Chukchi Basin (Figure 1b). A broad, seaward-
 127 dipping (ca. 0.3°) bathymetric depression (Western Bathymetric Trough) associated with the
 128 Herald Canyon on the Chukchi Shelf separates the western slope of the Chukchi Rise from the
 129 continental margin (Figure 1b). A similar bathymetric feature on the eastern side of the Chukchi
 130 Rise has been named the Broad Bathymetric Trough by Dove et al. (2014). Both troughs are
 131 characteristically short and wide (Western Bathymetric Trough ~20–60 km long and 150 km
 132 wide) unlike the well-developed cross-shelf troughs on the Arctic continental margins (e.g., Bear
 133 Island and M’Clure Strait troughs in Batchelor & Dowdeswell, 2014).

134 Multiple glaciogenic sediment accumulations and submarine landforms, such as mega-
 135 scale glacial lineations (MSGL), moraine ridges, and iceberg plowmarks, were identified by the

136 recent geophysical surveys on the Chukchi Borderland (Dove et al., 2014; Hegewald & Jokat,
137 2013; Ilhan & Coakley, 2018; Jakobsson et al., 2005, 2008; Polyak et al., 2001, 2007) and the
138 East Siberian margin (Joe et al., 2020; Niessen et al., 2013). These seafloor features were
139 interpreted to have been formed by grounding of several-hundred-meters thick ice caps and/or
140 ice shelves that impacted the Chukchi–East Siberian margin during several Quaternary
141 glaciations. The grounded ice masses on the Chukchi Borderland may have originated from the
142 Laurentide Ice Sheet to the east, the East Siberian margin to the west, and the Chukchi Shelf to
143 the south, possibly with the local ice-cap/ice-sheet covering the shallowest areas such as the
144 Chukchi Plateau (Dove et al., 2014; Jakobsson et al., 2005, 2008, 2014; Polyak et al., 2001,
145 2007) (Figure 1a). The deep-penetrating airgun seismic profiles across the shelf edge of the
146 Chukchi–East Siberian continental margin including the Chukchi Rise (purple and blue lines in
147 Figure 1b) show that the marine Neogene deposits on the outer shelf and slope are truncated by
148 glaciogenic sedimentary units downlapping on the pre-glacial strata (Dove et al., 2014;
149 Hegewald & Jokat, 2013; Ilhan & Coakley, 2018; Niessen et al., 2013). These stratigraphic
150 features indicate that large amounts of sediment were eroded by the grounded ice from the shelf
151 and transported to the slope. Based on the stratigraphic position of the resulting regional
152 unconformity within the Plio-Pleistocene deposits, the Chukchi continental margin has a long
153 glacial history (Hegewald & Jokat, 2013), but its timeline, patterns, and mechanisms involved
154 are still poorly understood.

155

156 **3 Materials and methods**

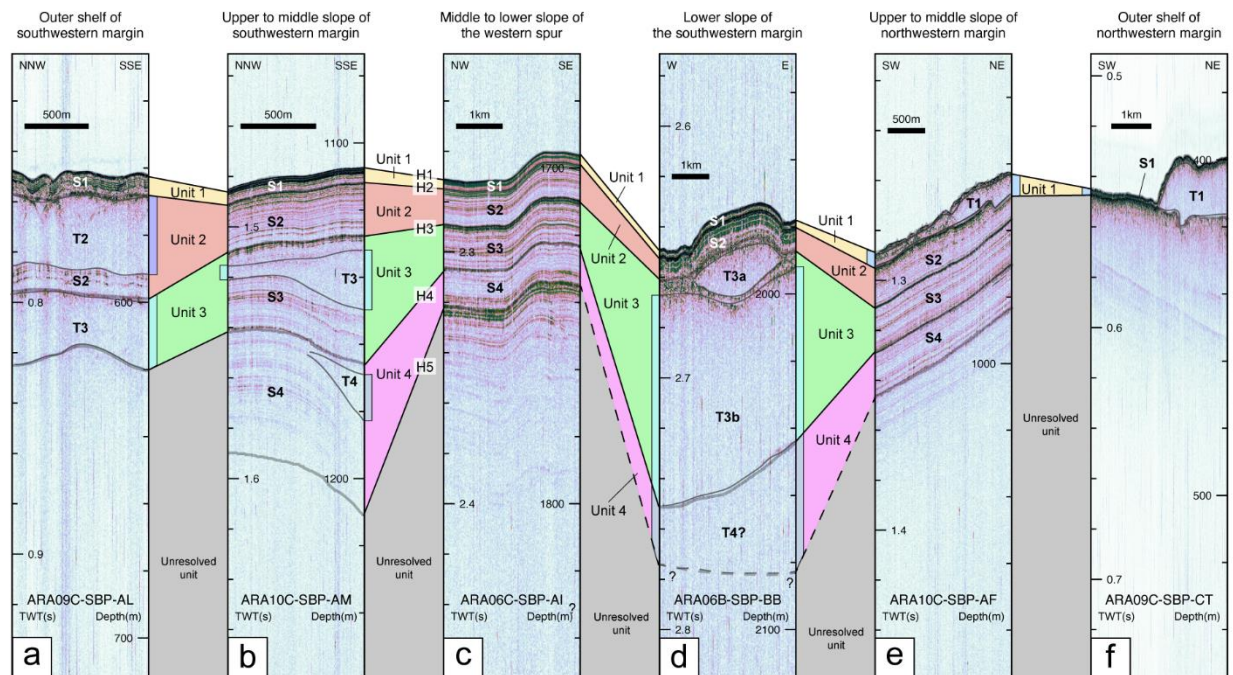
157 All of the new geophysical data used in this study were acquired by the 2015–2019 IBRV
158 *Araon* Arctic Expeditions ARA06B/06C, ARA07C, ARA09C, and ARA10C. These data fill a
159 coverage gap between regional geophysical data of the prior expeditions MGL1112 (Coakley et
160 al., 2011) and ARK-XXIII-3 (Jokat, 2009) (Figure 1b). For a broader regional coverage, we also
161 utilized the 2012 ARA03B data from the more northern and eastern parts of the Chukchi Rise
162 (Figure 1b). This paper is based primarily on the SBP and MBES data, with some of the airgun
163 seismic records used for verifying the identification of the major stratigraphic boundaries. The
164 frequency range of SBP data was set to 2.5–7.0 kHz with the ping rates of 1–2 s depending on
165 the water depth and recording window length (400–500 ms). These settings provided a sediment
166 penetration of tens of meters to less than 100 m, depending on the seabed morphology and
167 geological conditions, with a vertical resolution of ~0.5 m or better. During the ARA10C
168 SBP/MBES survey, the airgun seismic data were simultaneously collected using two Sercel
169 Generator-Injector (G.I.) guns (each 355 in³ volume; 250 in³ for generator and 105 in³ for
170 injector) and a 1.5-km-long Sercel Sentinel solid-type streamer (120 channels). The MBES
171 system recorded travel times and amplitudes of reflected signals with a wide beam angle (–65° to
172 +65°). The swath width of MBES data is ~4.3 times the water depth. The MBES bathymetry data
173 were frequently calibrated using the sound velocity profiles of the conductivity-temperature-
174 depth (CTD) castings. The MBES backscatter intensities were recorded simultaneously with the
175 bathymetry data acquisition. The quality of all data varied with the weather, sea ice conditions,
176 and ship speed.

177 The processing procedure applied to the SBP data includes delay-time shifting,
178 resampling, signal enveloping, spherical divergence correction using Seismic Unix. The
179 coordinates of each ping point number (PN) were extracted from the SBP data header. The

180 airgun seismic data were processed through conventional processing steps, including setup of the
 181 geometry, debubble, velocity analysis, multiple attenuation, pre-stack time migration, common
 182 mid-point stack, and seafloor muting using Schlumberger Omega 2017. The processed SBP and
 183 airgun seismic data were imported into the seismic data interpretation software SeisWare
 184 Geophysics for acoustic facies analysis, horizon picking, seismic correlation, and isopach
 185 mapping. The sediment depths were estimated from the two-way travel time using 1500 m/s
 186 sound speed. The resolved stratigraphic boundaries were traced on the SBP and airgun seismic
 187 data (Figures 2 and S1–S3). The identified seismostratigraphic units/subunits were gridded to a
 188 resolution of 100 m using a minimum curvature interpolation and were presented in the sediment
 189 thickness maps (Figure 3 and S4). The new, high-resolution MBES bathymetry and backscatter
 190 data were processed using CARIS HIPS&SIPS. The processed MBES results were gridded to a
 191 resolution of 20 m and were superimposed on the regional bathymetry grid (IBCAO V4;
 192 Jakobsson et al., 2020) using the QGIS software.

193

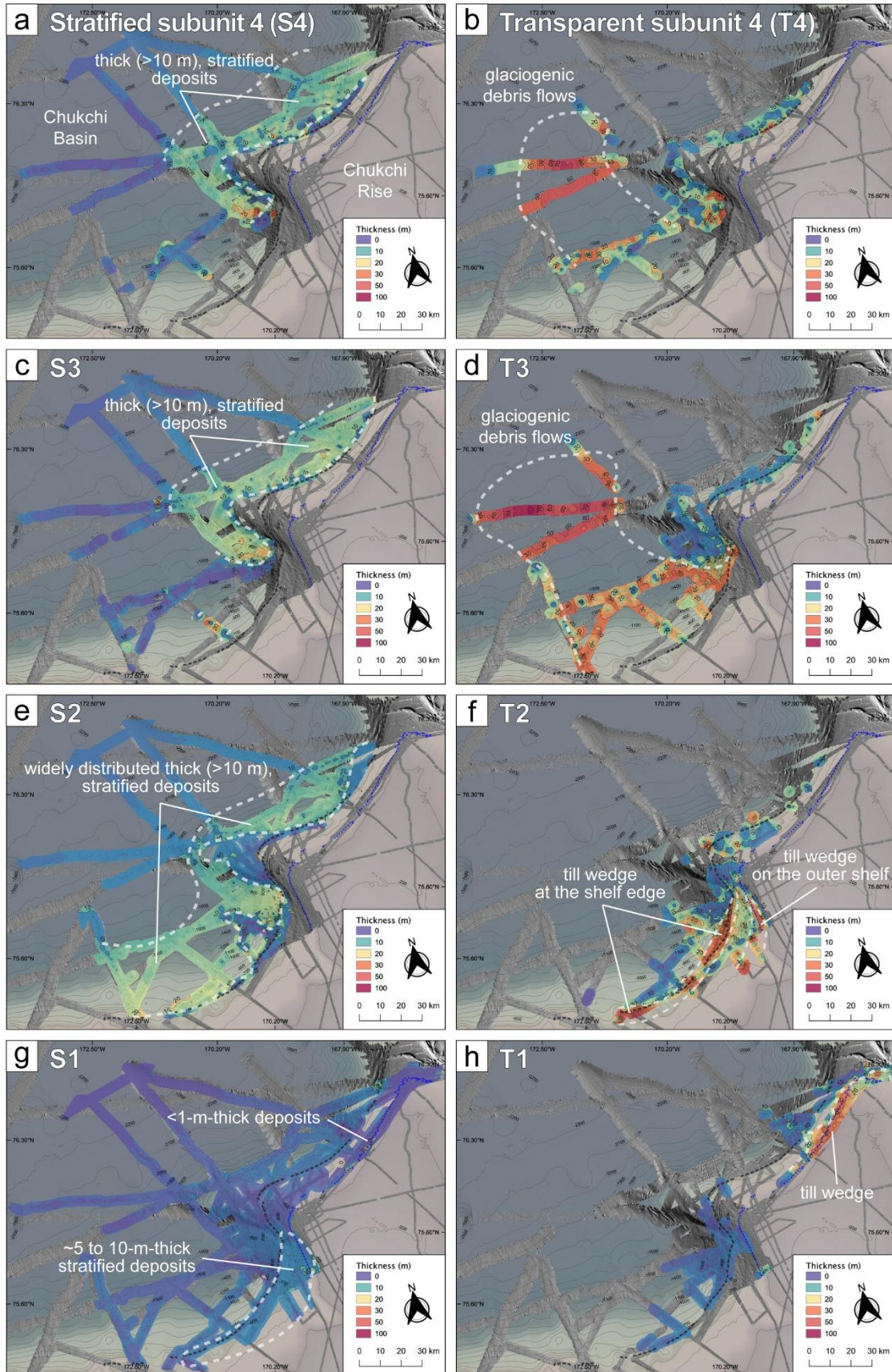
194



195

196 **Figure 2. (a)–(f)** The SBP data columns summarizing the seismic stratigraphy of the western
 197 Chukchi Rise margin. Seismostratigraphic units U4 to U1 are defined by the laterally continuous
 198 reflectors marked by thick gray solid lines. Depositional bodies (lenses) T4 to T1 are the
 199 acoustically transparent subunits (facies) within units U4 to U1. The location of the SBP
 200 columns *a–f* is shown in Figure 1b.

201



203 **Figure 3.** Sediment thickness maps of the acoustically stratified subunits S4 to S1 (**a, c, e, g**) and
 204 the acoustically transparent subunits T4 to T1 (**b, d, f, h**) on the outer shelf and slope of the
 205 western Chukchi Rise. The hillshaded multibeam bathymetry data is shown in gray-tones on the
 206 regional bathymetry. The sediment thickness was converted from milliseconds to meters at 1500
 207 m/s sound velocity. The lower boundaries of S4 and T4 on the mid-lower southwestern slope
 208 were partially defined in the SBP data (Figure 4), the thickness of S4/T4 is tentatively plotted in
 209 Figures 3a and 3b.

210

211

212 **4 Results**

213 4.1 Seismostratigraphy

214 The SBP data show the stratal geometries, internal structures, stacking patterns, and
 215 stratigraphic relationships in the uppermost, mostly ~20–40-m-thick deposits. The covered
 216 sedimentary succession was divided into four major seismostratigraphic units designated as U4
 217 to U1 from the oldest to the youngest (Figures 2 and S4). The unit boundaries were identified by
 218 erosional unconformities and/or otherwise laterally sub-continuous, high-amplitude seismic
 219 reflections H1–H5 (where H1 is a seafloor) in both of the SBP and accompanying airgun seismic
 220 records (Figures 2 and S1–S3). These reflectors have the best expression at the foot of the
 221 western Chukchi Rise slope, from where they were traced up-slope using the key SBP lines
 222 (Figure S1). Although the SBP grid in the northwestern area is relatively sparse, a consistent
 223 stacking pattern of the identified units and their mostly continuous boundaries enable the
 224 seismostratigraphic interpretation for most of the western Chukchi Rise margin (Figures 2, 3, and
 225 S1).

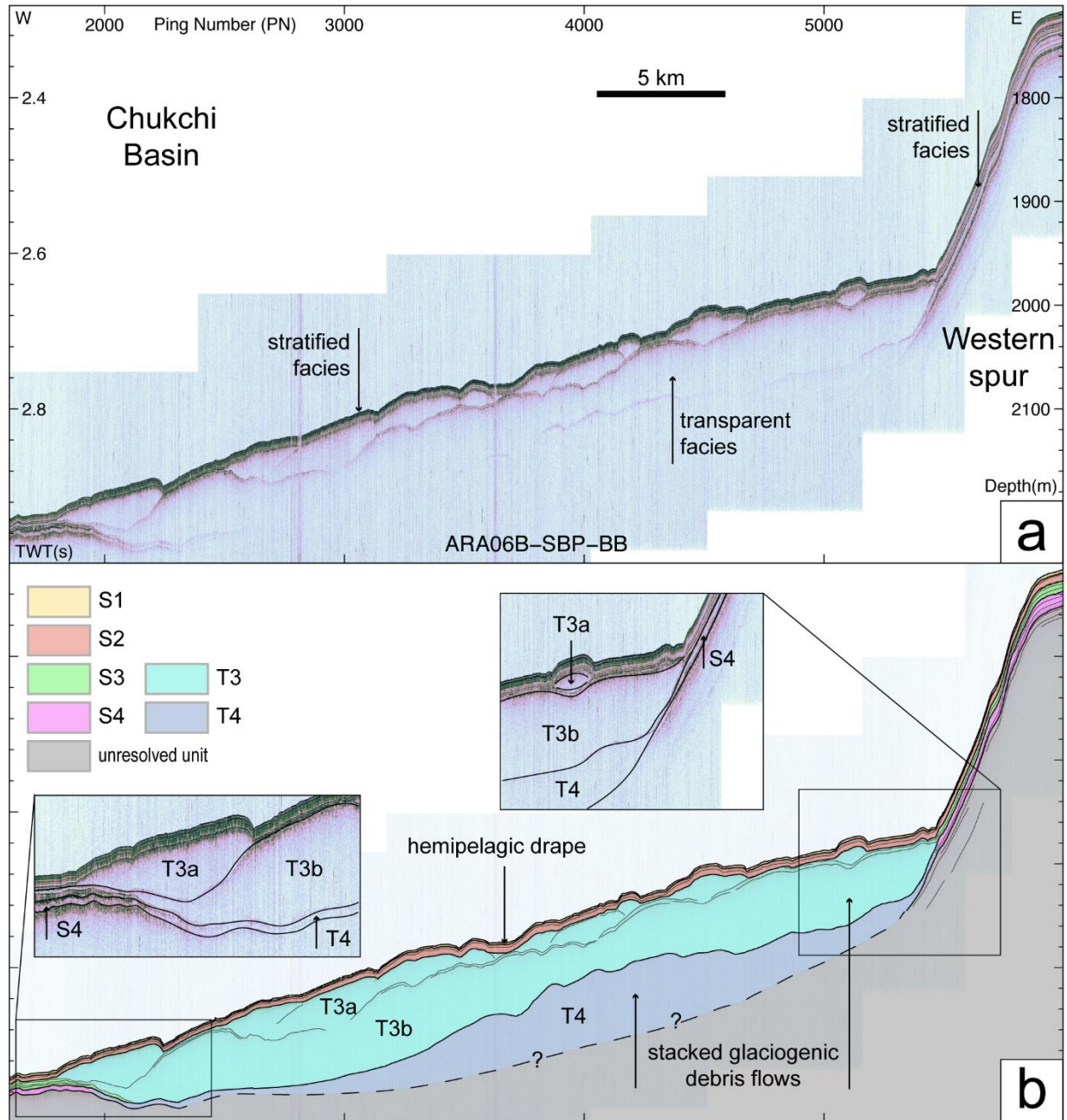
226 Each major unit is composed of two seismostratigraphic facies (subunits). One is
 227 acoustically stratified and shows parallel to subparallel internal configuration, high-to-medium
 228 lateral continuity, and low-to-medium amplitude reflections (Figure 2). The stratified subunits,
 229 S4–S1, mimic a smooth or undulated geometry of the underlying unit boundaries in most of the
 230 study area (Figures 2b, 2c, and 2e). The other facies type is distinguished in lens- or sheet-shaped
 231 deposits with a transparent/semi-transparent acoustic signature (Figure 2). The lower boundary
 232 of the transparent subunits, T4–T1, typically truncates the internal reflections or the underlying
 233 units (Figure 2a–2e and 2f). These boundaries correspond to the main reflectors between the
 234 units, otherwise the upper and lower boundaries of the transparent subunits pinch out and
 235 continue as internal reflections (Figures 2b, 2d, and 2f). The constructed isopach maps show the
 236 distribution of sediment thickness of the identified stratified subunits S4 to S1 and transparent
 237 subunits T4 to T1 (Figure 3). Below we describe these stratigraphic divisions from bottom to top.

238 4.1.1 Unresolved strata

239 The oldest deposits captured by the SBP records are represented by the stratigraphically
 240 unresolved strata with subparallel internal reflections. At the mid-lower slope of the
 241 southwestern Chukchi Rise, the unresolved strata show a stacking pattern similar to the overlying
 242 units U4–U1 (PN 5300–6000 in Figure 4 and PN 3000–6000 in Figure 5). In contrast, on the
 243 outer shelf of the western Chukchi Rise, the SBP data show that wavy, subparallel internal
 244 reflections of stratigraphically unresolved lower strata are truncated by the base of the major

245 units and subunits (PN 3500–4500 in Figure 6 and PN 2000–12000 in Figure 7). These records
 246 are similar to the wavy, continuous reflections that are overlain by the thick package of
 247 glaciogenic sediments along the slope of the Chukchi margin as shown by the prior and
 248 ARA10C airgun seismic data (Dove et al., 2014; Hegewald & Jokat, 2013; Ilhan & Coakley,
 249 2018) (Figures 1 and S3).

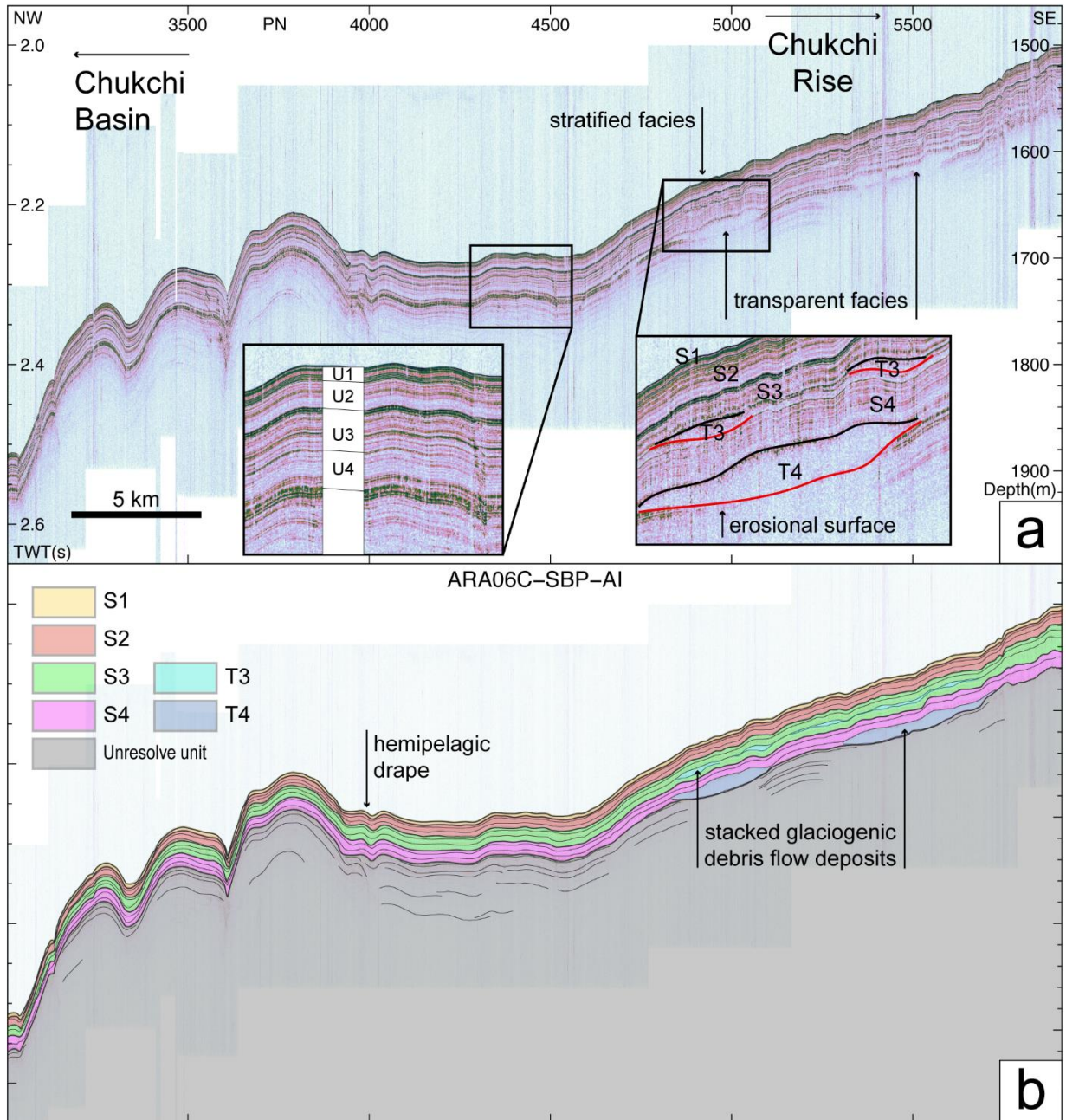
250
 251



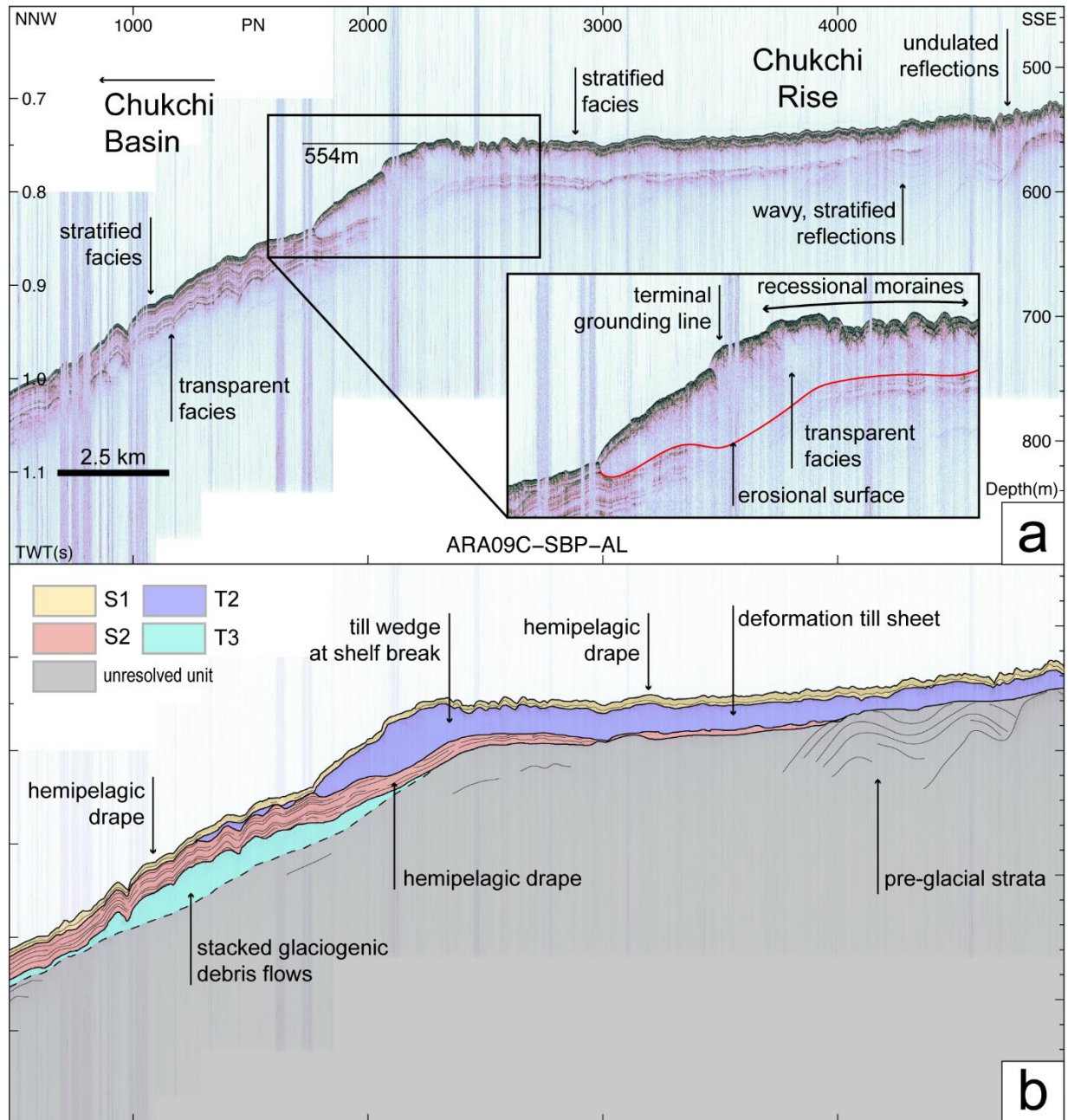
252

253 **Figure 4.** Uninterpreted (a) and interpreted (b) sub-bottom profile ARA06B-SBP-BB extended
 254 into the Chukchi Basin (see Figure 1b for location). The SBP data show stacked glaciogenic

255 debris lobes of acoustically transparent subunits T4 and T3 interbedded with acoustically
 256 stratified subunits S4–S1. Vertical axes are two-way travel time in the left and depth in meter at
 257 1500 m/s sound speed in the right.
 258
 259
 260



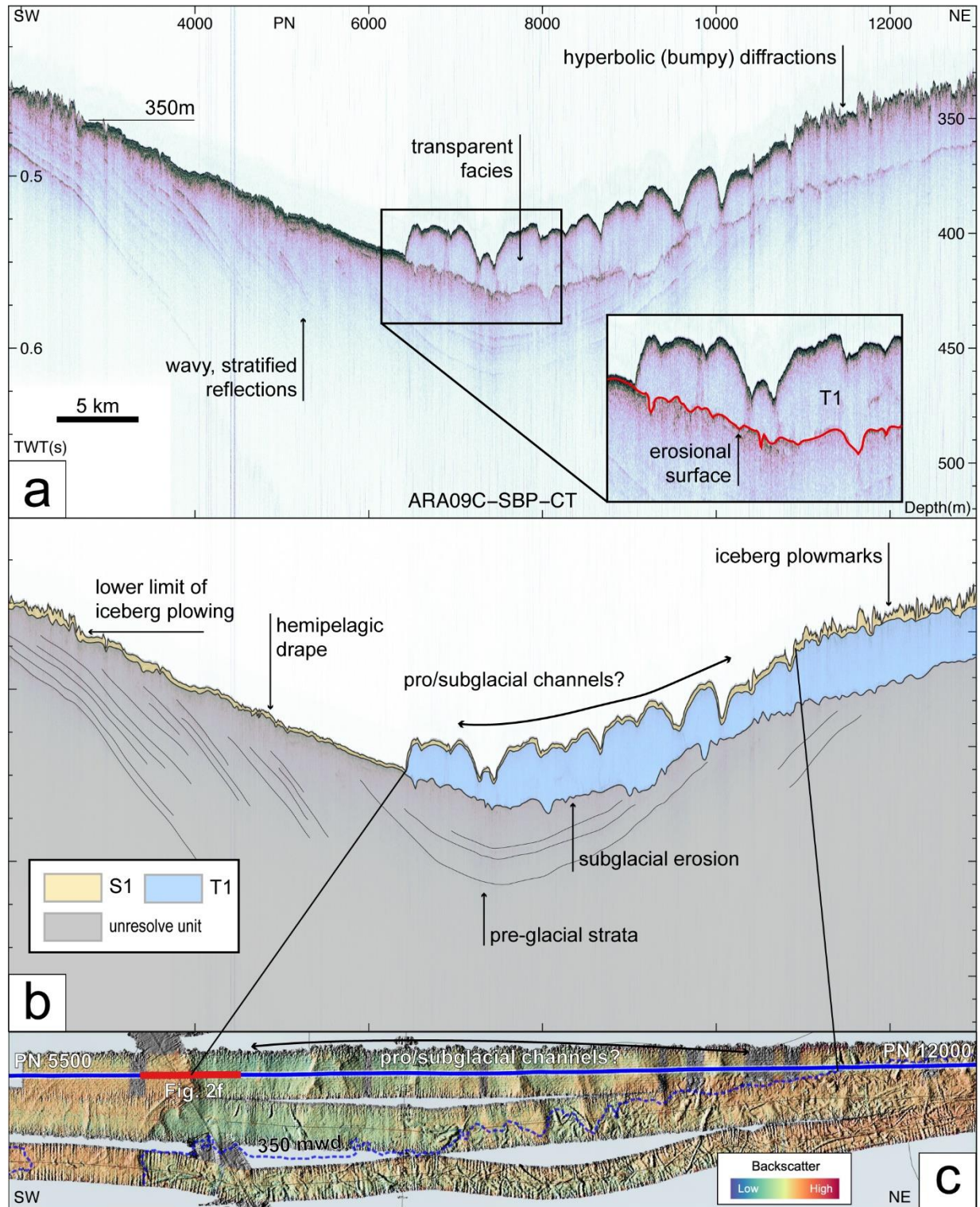
261
 262 **Figure 5.** Uninterpreted (a) and interpreted (b) sub-bottom profile ARA06C-SBP-AI showing
 263 acoustically transparent T4 and T3 lenses within acoustically stratified sediments of S4 to S1 on
 264 the middle to lower southwestern slope (see Figure 1b for location).
 265
 266



267

268 **Figure 6.** Uninterpreted (a) and interpreted (b) sub-bottom profile ARA09C-SBP-AL showing
 269 acoustically transparent deposits T2 and T3 interbedded with acoustically stratified sediments on
 270 the southwestern outer shelf to upper slope (see Figure 1b for location).
 271

272



273

274 **Figure 7.** Uninterpreted (a) and interpreted (b) shelf-edge parallel sub-bottom profile ARA09C-SBP-CT at the northwestern shelf (see Figure 1b for location). The surface of the acoustically
 275 transparent deposit T1 features pro- or subglacial channels and iceberg plowmarks at water
 276

277 depths below and above 350 m, respectively. (c) MBES backscatter intensity on the top of T1.
 278 Red to blue colors show higher to lower backscatter intensity, respectively.

279
 280

281 *4.1.2 Seismostratigraphic unit U4*

282 The mapped distribution of U4 shows that a thick (>10 m) stratified portion of the major
 283 unit, S4, is widely developed along the upper-mid slope of the western spur and the northwestern
 284 margin of the Chukchi Rise (white dashed outlines in Figure 3a). The transparent subunit T4 is
 285 characterized by ~5 km wide, 10–20-m-thick accumulations along the upper-mid slope of the
 286 margin at water depths of 600–1700 m (Figure 3b). These transparent sediment bodies are
 287 intercalated with acoustically stratified sediments (Figure 3b and PN 4800–5800 in Figure 5).
 288 Defining the full thickness of the S4 and T4 deposits on the mid-lower southwestern slope is
 289 mostly not possible because most of the lower unit boundaries here are not reached by the SBP
 290 data (Figure 2d and PN 2300–5300 in Figure 4). Based on the partially observed lower
 291 boundaries of S4 and T4 (PN 1800–2300 and 5400–5500 in Figure 4), we determine the
 292 thickness of the S4 and T4 deposits as <10 and ~20–70 m, respectively (Figures 3a and 3b). The
 293 upper part of U4 in this area shows a distinct lens-shaped, transparent deposit of T4 (Figures 2d
 294 and 4). The overall distribution of U4 is restricted to water depths deeper than 600 m (black
 295 dashed line in Figures 3a, 3b, and S4a), being possibly eroded at shallower depths, where
 296 younger deposits of U2/U1 rest directly on the erosional surface of the unresolved older strata
 297 (Figures 6 and 7).

298 *4.1.3 Seismostratigraphic unit U3*

299 The stratified subunit S3 are mostly observed on the continental slope of the northwestern
 300 margin and the western spur (Figure 3c), whereas the transparent subunit T3 occupies the
 301 southwestern margin at water depths of 550–2100 m (Figure 3d). A 10–20-m-thick accumulation
 302 of S3 (white dashed outline in Figure 3c) partially intercalated with transparent lenses of T3
 303 occurs beyond the present-day shelf break (Figure 3d and PN 4800–5000 in Figure 5), similar to
 304 the underlying U4 deposits. T3 shows the highest accumulation (>30 m thick, ~70 km wide,
 305 white dashed outline in Figure 3d) on the lower slope of the southwestern margin at water depths
 306 of 1800–2100 m (Figures 2d and 4). This depocenter can be divided into two depositional bodies
 307 interbedded with stratified sediments (Figures 2d and 4b). The upper subunit T3a shows a lens-
 308 shaped external geometry and a relatively restricted distribution, whereas, the lower subunit T3b
 309 is larger both laterally and vertically and has irregular or sheet-like external geometry (Figure 4).
 310 This distinctive stacking pattern of T3 can be observed from the upper to the lower slope of the
 311 southwestern Chukchi Rise. T3b is separated from irregularly shaped T4 deposits by a
 312 discontinuous, weak reflection (PN 2000–5000 in Figure 4). This faint reflection correlates with
 313 the U4/U3 unit boundary in the Chukchi Basin (PN 2000 in Figure 4) and on the lower slope of
 314 the western spur (PN 5500 in Figure 4), where acoustic facies are well stratified. On the
 315 southwestern outer shelf and upper slope, T3 has a high-amplitude, sub-continuous upper
 316 boundary, and a less distinct lower boundary (PN 500–2000 in Figure 6).

317 *4.1.4 Seismostratigraphic unit U2*

318 A thick (>10 m) stratified subunit S2 is widely developed along the slope of the
 319 northwestern margin and the western spur and extends to the southwestern margin of the

320 Chukchi Rise (white dashed outline in Figure 3e). S2 thins out in a basinward direction and
321 reaches a thickness of <10 m in the lower slope (Figure 3e). The internal S2 reflections are
322 generally subparallel to the lower unit boundary of U2 on the mid-lower slope of the
323 southwestern margin and most of the slope at the northwestern margin and the spur (Figure 5).

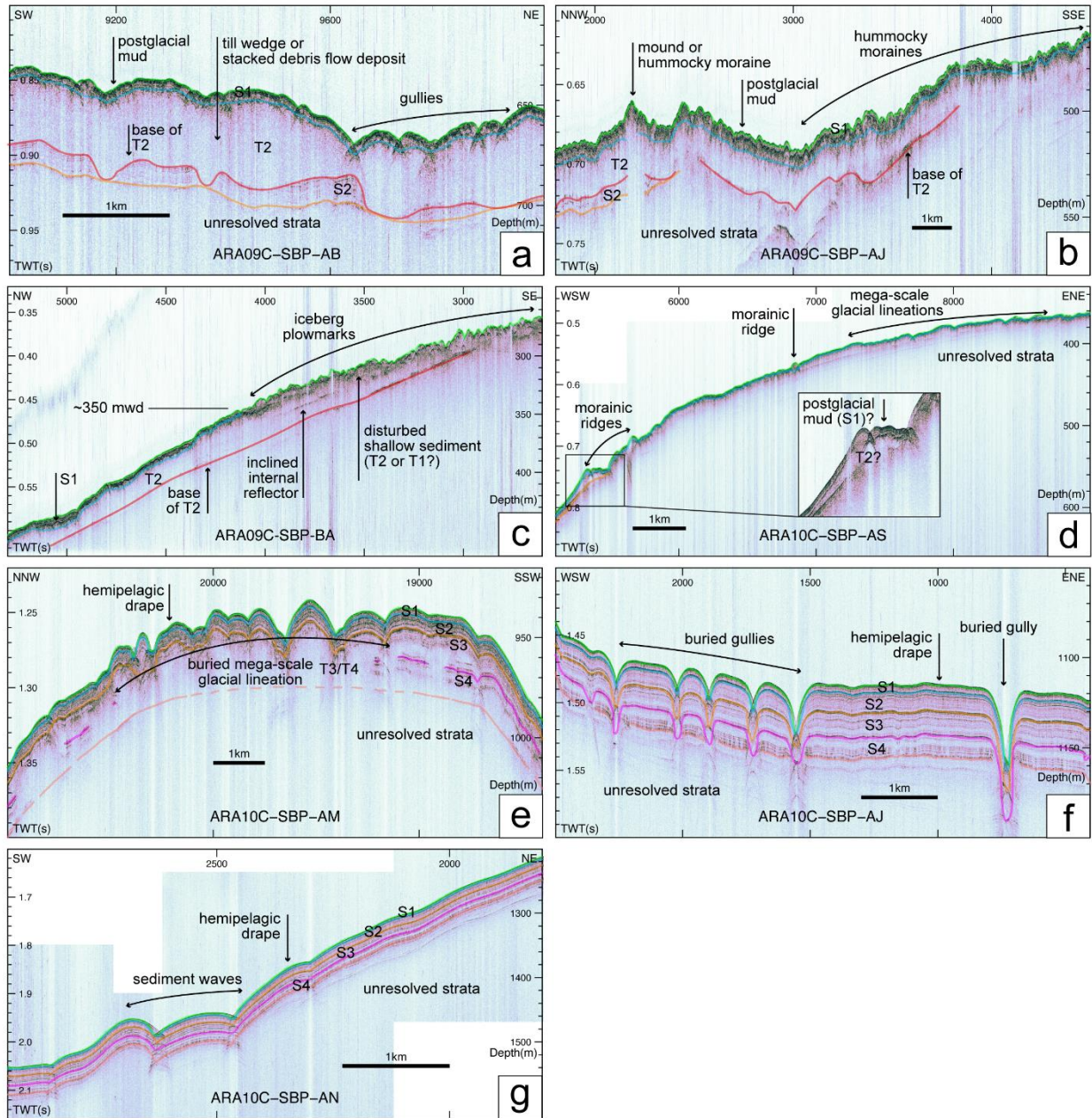
324 The main distribution of T2 shows a >20-m-thick, elongated sediment wedge (Figure 6)
325 extending to >80 km along the shelf edge at water depths of 520–640 m (white dashed outline at
326 the shelf edge in Figure 3f) with a downslope extension of debris lobes to 800 mwd (Figure 8a).
327 The wedge at the shelf edge has an uneven lower boundary truncating the stratified internal
328 reflections of the underlying sediments (PN 1700–3000 in Figure 6). The wedge surface is
329 irregular, and the boundary with the overlying stratified sediments of S2/S1 is distinct on the
330 upper slope and shelf edge but gets disturbed further shelfward (PN 4200–5000 in Figure 6 and
331 Figure 8b). Another >20-m-thick, elongated wedge of a similar deposit occurs further shelfward
332 at 300–450 m depths (white dashed outline at the inner shelf in Figure 3f). The stratigraphic
333 relationship between these adjacent deposits is not completely clear, but the presence of an
334 inclined internal reflector (PN 3300–4000 in Figure 8c) indicates that the wedges probably
335 belong to separate depositional events.

336 A spatially smaller but comparably thick depocenter attributed to T2 is observed on the
337 middle southwestern slope at water depths of 1200–1450 m (Figure 3f). Minor portions of T2 are
338 also distributed on the outer shelf and upper slope of the western spur and the northwestern
339 margin (Figure 3f).

340 *4.1.5 Seismostratigraphic unit U1*

341 The uppermost seismostratigraphic unit U1 features an overall thin (<10 m) stratified
342 subunit S1 along most of the western Chukchi Rise margin (Figure 3g). U1 thins from 5–10 m on
343 the outer shelf to just a couple of meters on the lower slope of the western margin (Figures 2a,
344 2c, 3g, and S4d). On the outer northwestern shelf, U1 directly overlies the eroded unresolved
345 strata (Figure 7). Transparent facies of T1 cannot be identified in the thin U1 deposits on the
346 mid-lower slope and rise (Figures 3h, 4, and 5), but show a >20-m-thick and >40-km-long
347 sediment wedge at the northwestern shelf edge at water depths of 310–420 m (Figure 3h). This
348 deposit overlies the unresolved strata with an uneven, erosional unconformity, whereas its
349 surface features high-amplitude incisions and furrows, and is covered by a thin (<1–2 m),
350 conformable sedimentary layer (PN 6200–13000 in Figure 7). Minor amounts of transparent
351 deposits occurring on top of the inner T2 wedge on the southwestern margin likely also belong to
352 T1 (PN 2600–4000 in Figure 8c). Thin S1 deposits are observed at <350-mwd throughout the
353 entire study area (PN 1850–2700 and 11000–13000 in Figure 7). The MBES backscatter data on
354 the U1 surface show a sharp intensity variation from –34 to –28 dB on the unresolved, old strata
355 to –42 to –38 dB on the subunit T1 (Figure 7c).

356



357

358 **Figure 8.** SBP data on the outer shelf to lower slope of the western Chukchi Rise (see Figure 9a
 359 for location). **(a)** Gullies on top of the transparent subunit T2 on the upper southwestern slope.
 360 **(b)** Mounds and hummocky moraines on the outer southwestern shelf. **(c)** T2 deposits on the
 361 southwestern shelf. A faint inclined internal reflector separates two till wedges (Figure 3f). **(d)**
 362 Morainic ridges and mega-scale glacial lineations (MSGL) on the outer shelf to upper slope of
 363 the western spur. **(e)** Buried MSGLs on the middle slope of the western spur. **(f)** Buried gullies
 364 on the northwestern upper-mid slope. Simultaneously acquired airgun seismic data is shown in
 365 Figure S2. **(g)** Buried sediment waves on the middle slope of the western spur.

366

367

368 4.2 Geomorphic features

369 The MBES bathymetry data provide three-dimensional geometry and detailed
370 morphological characteristics of submarine landforms related to various subglacial, ice-marginal,
371 glaciomarine, and open marine environments (Figures 9 and S5). In addition, the MBES
372 backscatter data can provide indirect characteristics of seabed such as grain-size composition,
373 sediment compaction, and seafloor roughness and hardness (Fransner et al., 2017; Huang et al.,
374 2018; Todd et al., 2007). As the hull-mounted MBES systems have a lower frequency range (12
375 kHz) than usual side-scan sonar systems (550 kHz to 1 MHz), the MBES backscatter data in this
376 study are more suitable for detecting differences in bulk density between young, soft muds and
377 older, consolidated sediments rather than grain size effects (Wille, 2005; Zaragosi et al., 2000).

378 Two sets of streamlined linear landforms are observed in the MBES bathymetry data on
379 the outer shelf and middle slope of the western spur (Figures 8d, 8e, and sky-blue lines in Figure
380 9a). The S–N trending, 5 to 12-km-long and 100 to 200-m-wide lineations on the outer shelf are
381 distributed across a 6-km-wide field at water depths of ~350 to 460 m (Figures 8d and 9a). At the
382 350-mwd limit, lineations are overprinted by the randomly oriented, curvilinear to sinuous
383 furrows 50 to 250-m-wide and <10-m-deep (short black lines in Figure 9a). Both the lineated and
384 furrowed areas have a rough relief appearing in the SBP data as diffraction hyperbolas (e.g., PN
385 11000–13000 in Figure 7a and PN 7200–8700 in Figure 8d). These areas also feature relatively
386 high MBES backscatter of –32 to –28 dB (red-colored field in Figure 9a) and only very thin
387 sediment cover on top (PN 7200–8700 in Figure 8d). The other lineation set features SSW–NNE
388 trending linear features 4 to 7-km-long and 180 to 400-m-wide at water depths of 780 to 940 m
389 on the middle slope (PN 19100–20300 in Figure 8e and Figure 9a). These lineations are formed
390 on top of the transparent subunits T3/T4 and are overlain by 10 to 15-m-thick acoustically
391 stratified sediments S1/S2 with low backscatter intensities of –42 to –34 dB (Figures 8e and 9a).

392 Mostly bathymetry-parallel, nested, curvilinear to sinuous ridges are observed along the
393 shelf edge between 410 and 550-mwd of the western spur and the southwestern Chukchi Rise
394 margin (Figure 8d and blue lines in Figure 9a). Potentially similar, but shorter and sparser
395 features occur on the outer shelf of the southwestern margin, in the area of a >3-km-wide
396 bathymetric terrace (Figure 9a). The ridges on the western spur are 3–6-m-high and >50-km-long
397 along the shelf edge (Figure 9a). The deepest ridge on the western spur shows an asymmetric
398 geometry and is covered by a ~3-m-thick stratified sediments of S1 (inset in Figure 8d). The
399 sparser ridges on the southwestern outer shelf are ~3–5-m-high and ~3–7-km-long (Figure 9a).
400 They are positioned on top of the undulated surface of T2 and are overlain by the stratified
401 sediments of S1 (PN 2200–2700 in Figure 6).

402 Mound-shaped bedforms with transparent acoustic facies are observed on the upper slope
403 and the outer shelf terrace of the southwestern margin at water depths of 600–700-m (inside
404 white dashed outlines in Figure 9a). The mounds are aligned subparallel to the boundary between
405 the western spur and the shelf edge terrace (Figure 9a). Eight mounds surveyed on the upper
406 slope have widths of 200–700 m and are ~10 m higher than the surrounding seafloor (Kim et al.,
407 2020). Larger scale mounds observed on the shelf edge terrace extend stratigraphically to the
408 U2/U1 unit boundary (PN 2100–2500 in Figure 8b and Figure 9a).

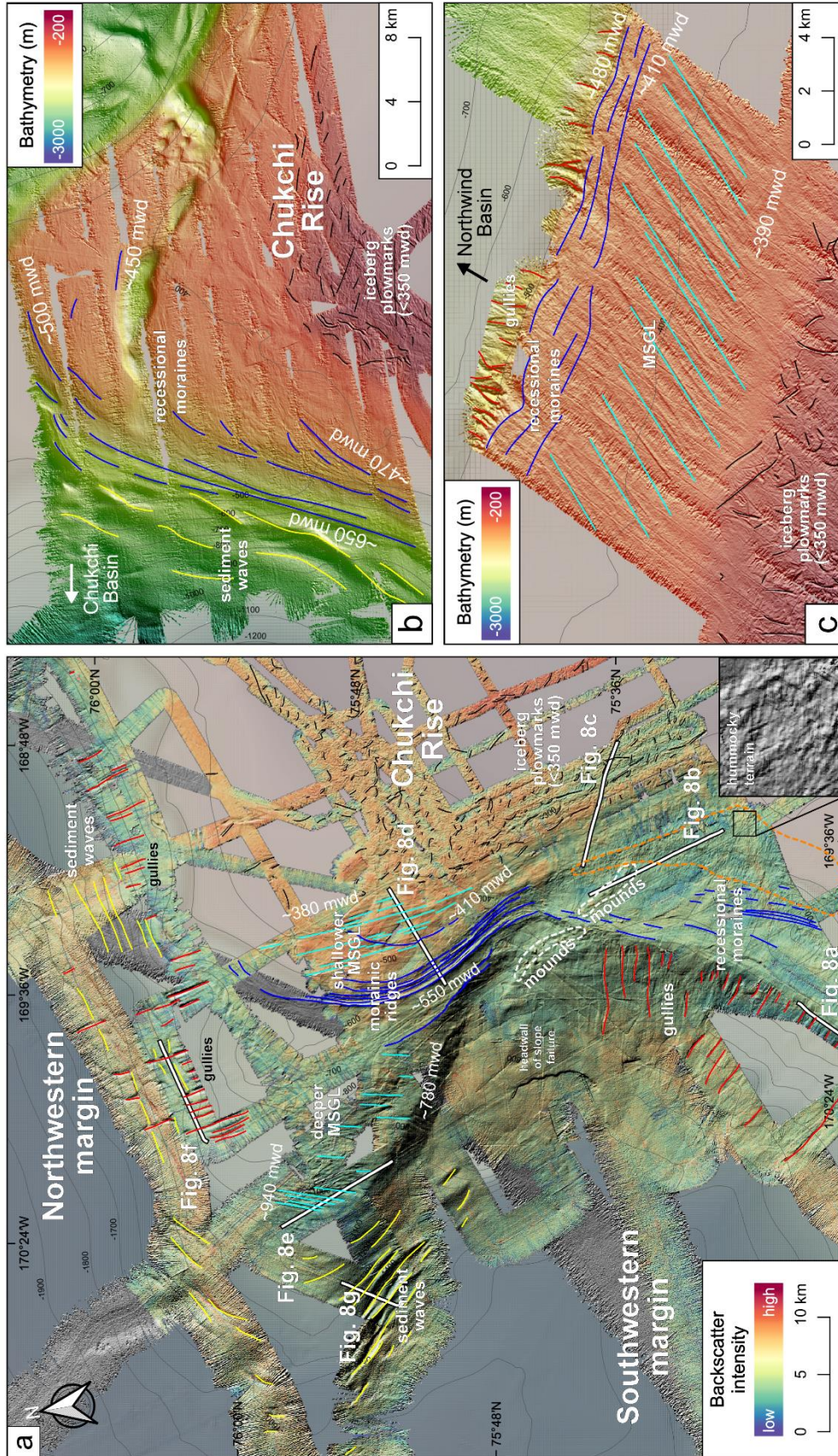
409 A field of slightly elongated to nearly circular small mounds (hummocks) is located ~5
410 km shelfward from the shelf break at the southwestern margin at water depths of 440–540 m
411 (inside orange-dashed outline and lower right inset in Figure 9a). This hummocky terrain shows

412 gentle undulations (<10 m high) and a low-to-moderate linearity. The sediments composing
413 these bedforms belong to the transparent subunit T2 covered by stratified sediments of S1 (PN
414 3000–4500 in Figure 8b).

415 Narrow, ~100 m wide, depressions (incisions) in a dip direction are observed along the
416 western Chukchi Rise margin beyond the present-day shelf break at water depths of 600–1600 m
417 (red lines in Figure 9a). The incisions on the southwestern margin are developed on top of the
418 transparent subunit T2 and are covered by ~6-m-thick sedimentary layer S1 (Figure 8a). The
419 depths of these features decrease from ~10–20 m on the shelf break to <10 m on the mid-lower
420 slope. The upper slope incisions disappear on the western spur and are observed again on the
421 northwestern margin (Figure 9a). The latter features of ~20–30-m deep and ~400–500-m wide
422 show a more apparent, less sinuous geometry than on the southwestern slope. A thick (~50 m)
423 acoustically stratified sediment with diffraction hyperbolae covers the area with these incisions
424 (PN 700–800 and 1500–2400 in Figure 8f and Figure S2). Some dip incisions ~7–15-m deep and
425 ~500–1000-m wide were found on the outer shelf of the northwestern margin at 370–400-mwd
426 by the narrow stripes of the MBES data (Figure 7c). The SBP data show that these incisions are
427 developed on top of the transparent subunit T1 (PN 6200–11000 in Figures 7).

428 Distinctive undulated seafloor features elongated parallel to the bathymetry are observed
429 in the unresolved strata on the middle slope (1300–1600 mwd) at the western spur and the
430 northwestern Chukchi Rise margin (yellow lines in Figures 9a). On the northern slope, these
431 undulated features are cut by downslope incisions (Figures 8f and 9a). A thick (>20 m) stratified
432 sedimentary succession of U4 to U1 conformably overlies the undulating surface (Figure 8g).

433



434

435 **Figure 9. (a)** Interpreted submarine landforms drawn on the MBES backscatter map overlapping
 436 the hillshaded MBES bathymetry map (see Figure S5 for uninterpreted MBES bathymetry
 437 image). The interpreted morphological features, which were formed under subglacial, ice-
 438 marginal, and glaciomarine sub-environments, are marked by differently colored lines and labeled
 439 for the explanation. Inset in the lower right corner shows an enlarged view of the hummocky
 440 terrain (black box). Labeled white lines show the location of the SBP data in Figures 8a to 8g.
 441 Ancillary MBES bathymetry data (ARA03B) from the northern **(b)** and eastern **(c)** parts of the
 442 Chukchi Rise (see Figure 1b for location).

443

444

445 **5 Discussion**

446 5.1 Origin of identified sedimentary/geomorphic features

447 5.1.1 Seismostratigraphic units and facies

448 The major seismostratigraphic boundaries usually indicate either pronounced change in
 449 sedimentary environments or depositional unconformities (Veeken & van Moerkerken, 2013).
 450 On the glaciated shelves, including the study region (e.g., Dove et al., 2014; Hegewald & Jokat,
 451 2013; Niessen et al., 2013), these features were shown to be characteristically related to the ice-
 452 sheet dynamics and associated sedimentary/geomorphic processes. In addition to the direct
 453 erosion and deposition by grounded ice, high-amplitude, continuous reflectors commonly occur
 454 in glaciomarine environments in connection with massive deposition of iceberg-rafted debris
 455 (IRD) during glacial events (Gulick et al., 2017; Joe et al., 2020). In particular, a sediment core–
 456 seismic correlation in the western part of the Chukchi Basin indicates that strong reflectors in the
 457 SBP data correspond to the prominent, IRD-rich, detrital carbonate layers related to pulses of
 458 iceberg discharge from the Laurentide Ice Sheet (Joe et al., 2020).

459 Seismostratigraphic units/subunits encompassed by the resolved boundaries can be
 460 discriminated by the acoustic signature, such as stratified vs. transparent facies (Figure 2).
 461 According to previous lithostratigraphic studies, the Quaternary sediments in the western Arctic
 462 Ocean outside of the glacially impacted areas mainly consist of fine-grained to sandy muds with
 463 cyclic interlamination of brown and yellow to greyish intervals (e.g., Matthiessen et al., 2010;
 464 Schreck et al., 2018; Stein et al., 2010). This stratigraphy has been correlated with acoustically
 465 stratified facies similar to subunits S4–S1 in areas adjacent to this study area (Dove et al., 2014;
 466 Joe et al., 2020; Polyak et al., 2007). A detailed sedimentologic analysis in the western part of
 467 the Chukchi Basin indicated that the stratified facies had been formed by suspension settling of
 468 turbid meltwater plumes and detached turbid layers during glaciation/deglaciation and by
 469 hemipelagic settling during the interglacial periods (Joe et al., 2020). The interpretation is
 470 consistent with multiple studies of ice distal glaciomarine sediments (e.g., C. H. Eyles et al.,
 471 1991; Ó Cofaigh et al., 2003). In comparison, the transparent deposits (e.g., subunits T4–T1 in
 472 Figure 2) indicate lenses of acoustically homogenous sediments without internal bedding due to
 473 fast deposition or internal deformation, which is especially common under pro- or subglacial
 474 conditions (Alley et al., 1986; Dowdeswell et al., 2004; Gulick et al., 2017). Resulting deposits
 475 are seen in the seismic profiles as sheet- or wedge-shaped, acoustically transparent bodies
 476 usually interpreted as deformation tills (e.g., Dove et al., 2014; Ó Cofaigh et al., 2005). A similar

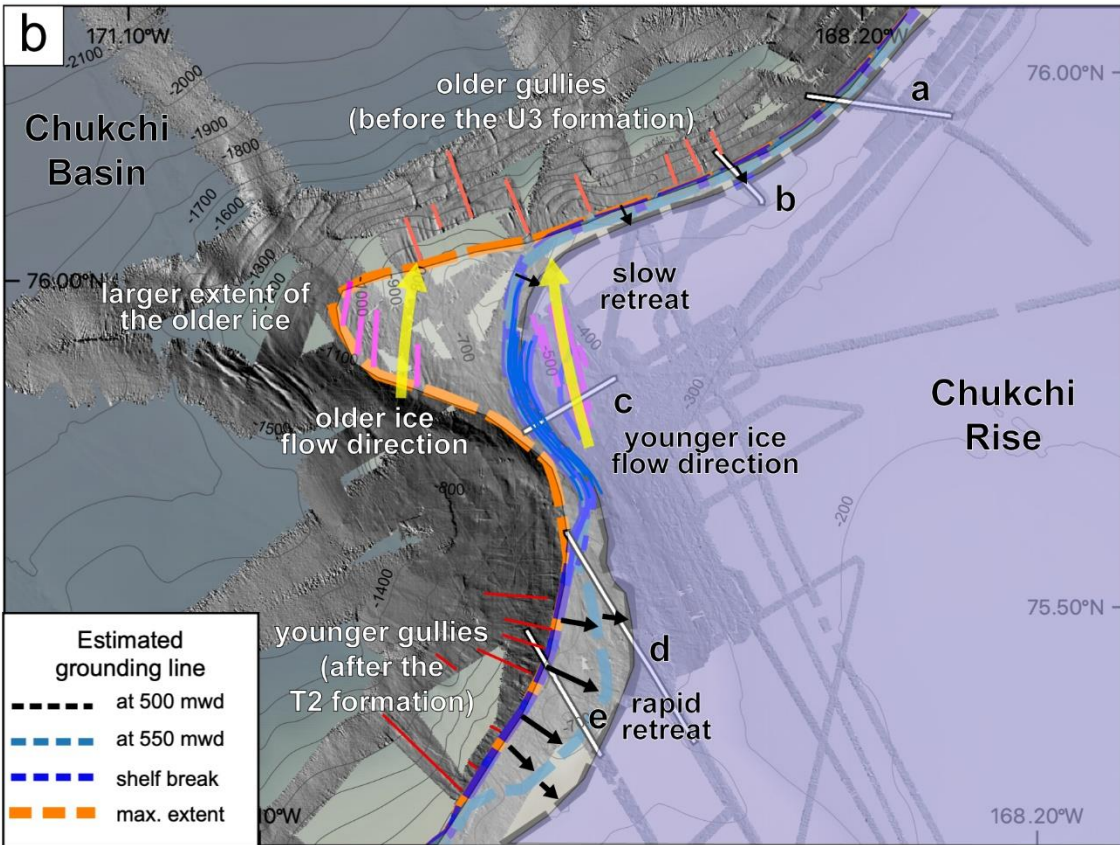
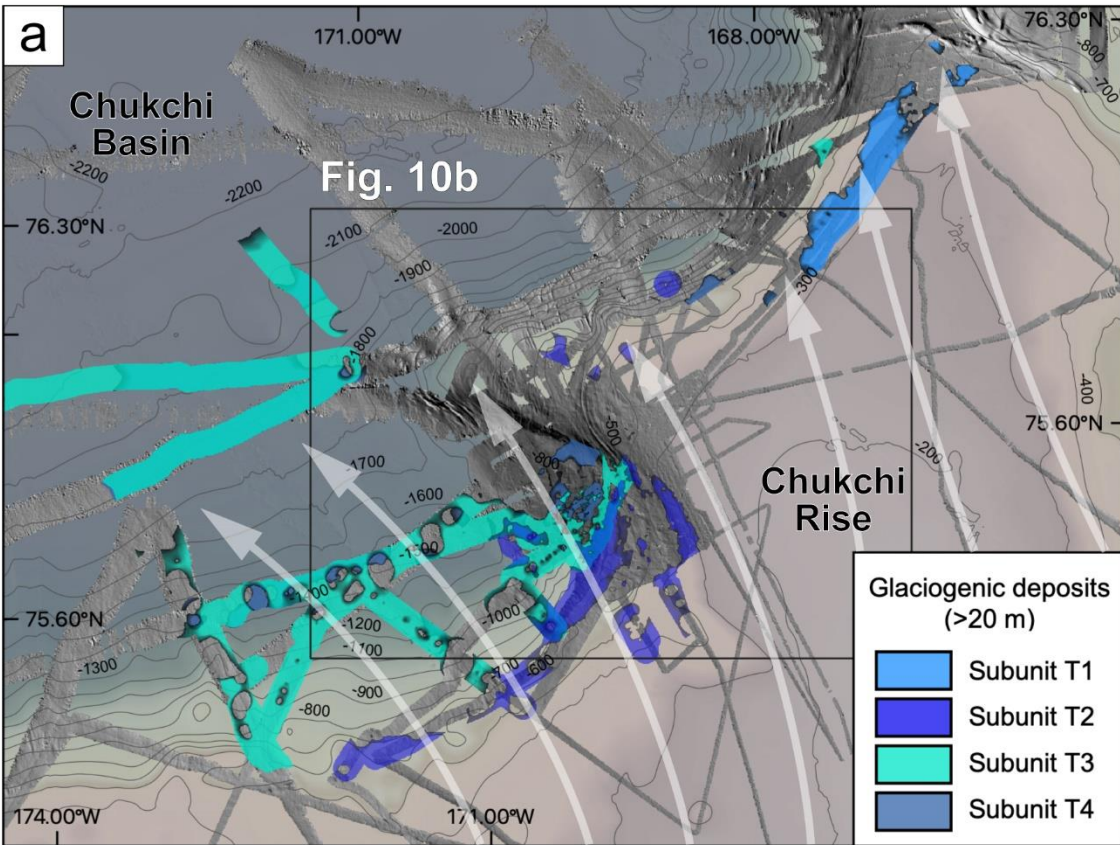
477 acoustic signature may also characterize deposits formed by episodic events like ice-sheet
478 bulldozing, debris flows, submarine landslides, or subglacial underwater flows during the ice-
479 sheet advances or early deglaciations (e.g., Donda et al., 2008; C. H. Eyles & Eyles, 2010; Gales
480 et al., 2016; Joe et al., 2020; Ó Cofaigh et al., 2003; Vorren & Laberg, 1997). However, these
481 short-lived events can hardly account for major, spatially continuous units.

482 Overall, sediment depocenters and stratal geometries of the acoustically transparent and
483 stratified sediments (Figures 3–7 and 10a) characterize glaciogenic sedimentary processes and
484 provide useful insights into past ice-sheet dynamics. The seismic stratigraphy of the transparent
485 deposits T4–T2 identified at the southwestern margin (Figures 4 to 7) corresponds to the
486 prograding foreset beds with an oblique tangential geometry reported for this area based on the
487 airgun seismic data (Dove et al., 2014; Hegewald & Jokat, 2013; Ilhan & Coakley, 2018) (purple
488 and blue lines in Figure 1b). The outer shelf to slope location, erosional bottom boundary,
489 wedge-shaped stacking pattern, and moderate lateral continuity of these foresets are consistent
490 with seismostratigraphic characteristics of glacial trough mouth fans (TMFs), diamicton-
491 dominated sediment accumulations typically formed at the cross-shelf glacial trough mouth
492 (Batchelor & Dowdeswell, 2014; Dowdeswell et al., 1996; Dowdeswell & Siegert, 1999; Laberg
493 et al., 2000; Ó Cofaigh et al., 2003; Vorren & Laberg, 1997). The occurrence of TMFs at the
494 southwestern Chukchi Rise margin indicates a large amount of sediment transferred by ice sheets
495 to the shelf edge and further down the slope over several glacial cycles. This depositional
496 environment reflects an extensive ice drainage from local or transiting grounded ice-sheets/ice-
497 shelves.

498 The location of the T4/T3 lens- or sheet-shaped depocenters on the mid-lower slope in
499 the TMF area (Figure 10a) suggests that they have been primarily formed by the glacially-fed
500 debris flows, whereas intercalated stratified facies likely indicate suspension settling from turbid
501 meltwater plumes (Figures 4 and 5). A similar picture has been reported for the East Siberian
502 slope across the Chukchi Basin from the study area (Joe et al., 2020; Niessen et al., 2013). Two
503 T3 subunits separated by the stratified sediments (Figure 4) indicate two depositional events
504 probably reflecting two glacial advances or deglacial pulses.

505 The T2 depocenter with an erosional basal boundary observed at the outer shelf to upper
506 slope of the Chukchi Rise is interpreted as a till wedge (Figures 6 and 10a). Similar deposits
507 composed of diamictons are typically formed at the stable grounding zones of ice sheets with
508 subglacial sediment transportation and deformation (e.g., Batchelor et al., 2018; Dove et al.,
509 2014; C. H. Eyles & Eyles, 2010; Ó Cofaigh et al., 2016). Based on the position of the large T2
510 till wedge, during the peak glaciation, the grounding zone was stretched along the shelf break at
511 the modern depths of 550 to 580 mwd (Figure 6; Figure 5 in Dove et al., 2014). A smaller till
512 wedge at depths of ~300–450 m on the southwestern inner shelf (Figures 8c and 10a) possibly
513 indicates another glacial event. The existing data, however, cannot resolve whether this deposit
514 corresponds to T2 or a younger transparent subunit T1. The distribution of the T1 depocenter
515 further north is limited to similar water depths not exceeding ~450 m (Figures 7 and 10a), which
516 suggests that this glaciogenic feature may correspond to the same glaciation. A more detailed
517 characterization of this deposit is not yet available due to a sparse data coverage at the
518 northwestern margin (Figure 1b), notably lacking the shelf-to-slope lines crossing the
519 depocenter.

520



521

522 **Figure 10. (a)** Spatial distribution of the acoustically transparent deposits T4 to T1 thicker than
 523 20 m. White arrows show major ice-flow trajectories inferred from the distribution of
 524 glaciogenic deposits T4 to T1 and related geomorphic features. The black rectangle indicates
 525 panel b. **(b)** Distribution of MSGL (purple lines with yellow arrows for the inferred direction),
 526 recessional morainic ridges (blue lines), and proglacial gullies (red lines). The orange dashed line
 527 indicates the inferred maximum extent of the grounded ice. Blue, sky blue, and black dashed
 528 lines are projected grounding lines at the present shelf break, 550 mwd, and 500 mwd,
 529 respectively. See also schematic cross-sections for grounding lines projections in Figure S6.
 530 Black arrows indicate retreats of grounding-line from the shelf break.

531

532

533 *5.1.2 Submarine landforms*

534 The randomly distributed, curvilinear to sinuous furrows abundant at water depths
 535 shallower than ~350 m (Figures 9a and 9c) are widely interpreted as iceberg plowmarks
 536 generated by the keels of free-floating icebergs under the glaciomarine environment (e.g.,
 537 Batchelor et al., 2018 and references therein). These features are ubiquitous at <~350-m depths
 538 at the outer continental margin from the Canadian Archipelago to East Siberia and the adjacent
 539 borderlands (e.g., Dove et al., 2014; Hunkins et al., 1962; Jakobsson et al., 2005, 2008, 2014;
 540 Polyak et al., 2001, 2007).

541 The long, streamlined landforms mapped in two areas of the western Chukchi Rise
 542 margin and the ancillary data (Figures 9a and 9c) are identified as mega-scale glacial lineations
 543 (MSGL), consistent with the interpretation in multiple studies from the glaciated margins
 544 (Dowdeswell et al., 2004; Ottesen et al., 2005). MSGL sets have been reported from multiple
 545 sites across the western Arctic Ocean margins and borderlands (Dove et al., 2014; Engels et al.,
 546 2008; Jakobsson et al., 2008, 2014, 2016; Niessen et al., 2013; Polyak et al., 2001, 2007). In
 547 general, these distinct directional features track the fast ice-stream flows, typically remained
 548 during ice-sheet collapses (e.g., Batchelor et al., 2018 and references therein).

549 By comparison with other glaciated seafloor areas, the bathymetry-parallel ridges at the
 550 shelf edge (Figure 9) can be interpreted as recessional moraines formed by the stepwise retreat of
 551 a grounded ice margin (Batchelor et al., 2017, 2018; Dove et al., 2014; Niessen et al., 2013;
 552 Ottesen & Dowdeswell, 2006; Polyak et al., 1997). The acoustically transparent facies of the
 553 identified ridges (inset in Figure 8d) indicate poorly sorted deposits, consistent with the diamict
 554 material typical for similar features (Bennett et al., 1996; Bradwell et al., 2008).

555 The mounds mapped on the southwestern upper slope (Figures 8b and 9a) are thought to
 556 be formed by the upward migration of gas/fluids, such as free gas from beneath the gas-hydrate
 557 stability zone (Kim et al., 2020). Such processes can be generated or reactivated by pressure and
 558 temperature changes in the deep strata caused by glacial isostatic rebounds during the grounded
 559 ice-sheet advances and retreats (e.g., Himmler et al., 2019).

560 The field of small mounds on the southwestern outer shelf has geomorphic and
 561 stratigraphic characteristics similar to hummocky moraines (Elvenes & Dowdeswell, 2016;
 562 Ottesen & Dowdeswell, 2009) (Figures 8b and 9a). Such landforms can be formed by stagnant
 563 ice pressing onto the soft deformable bed over large areas of sub-marginal and proximal

564 proglacial areas, including submarine environments (e.g., Batchelor et al., 2018 and references
565 therein; Boone & Eyles, 2001; N. Eyles et al., 1999).

566 The narrow dip incisions at the shelf edge and on the upper-mid slope (Figures 8a, 8f, and
567 9a) can be interpreted as gullies, which are commonly developed in front of the past ice
568 grounding lines (e.g., Engels et al., 2008; Gales, 2013; Rydningen et al., 2015). On the polar
569 continental margin, slope gullies can result from sustained cascading of cold waters (brines)
570 and/or sediment-laden subglacial meltwater flows (e.g., Anderson, 1999; Ivanov et al., 2004;
571 Lowe & Anderson, 2002; Noormets et al., 2009; Ó Cofaigh et al., 2018; Pope et al., 2018).
572 Broader incisions on top of the youngest transparent deposit T1 on the outer shelf (Figure 7c)
573 may represent valleys formed by the pro- or subglacial drainage during deglaciation (e.g.,
574 Stewart & Lonergan, 2011).

575 The regular undulations elongated along the slope in pre-glacial deposits (Figures 8g and
576 9a) appear like sediment waves formed by persistent along-slope bottom current (e.g.,
577 Miramontes et al., 2016). Similar features can also be identified in the airgun seismic records
578 from the Chukchi margin slopes in the pre-glacial deposits above the upper Miocene
579 unconformity (Hegewald, 2012; Hegewald & Jokat, 2013). A sandy composition of pre-glacial
580 sediments recovered on the northern Northwind Ridge corroborates a strong current activity at
581 the intermediate water depths (Dipre et al., 2018). In comparison, the subparallel stacking pattern
582 of the stratified facies S4 to S1 on top of the sediment waves (Figure 8g) indicates sedimentation
583 in quieter environments less affected by bottom currents (Veeken & van Moerkerken, 2013).

584

585 5.2 Development of glaciogenic deposits

586 5.2.1 Trough mouth fan contributions

587 Glaciogenic TMFs are typically formed in front of the cross-shelf glacial troughs -
588 elongated, landward deepening bathymetric depressions on the broad continental margins (e.g.,
589 Batchelor & Dowdeswell, 2014; Ó Cofaigh et al., 2003). The relatively narrow Chukchi Rise
590 extending offshore from the continental margin makes for a different geomorphic and
591 depositional environment. A slope gradient is considered as one of the principal factors that
592 control the development of TMFs (Batchelor & Dowdeswell, 2014; Ó Cofaigh et al., 2003). The
593 upper slope gradient of the southwestern Chukchi Rise margin is less than 4° (2–3° average)
594 (Figure 1b), which is suggested to be close to a limit of an effective accumulation of glaciogenic
595 material on the slope (e.g., Batchelor & Dowdeswell, 2014; Piper et al., 2012). Nevertheless, this
596 gradient is considerably higher than 1°, which allows for well-developed TMFs such as on the
597 Polar North Atlantic margins (e.g., Ó Cofaigh et al., 2003; Piper & Normark, 2009; Rydningen et
598 al., 2015). The acoustically transparent sediment depocenters of subunits T4 and T3 on the
599 southwestern middle to lower slope (Figures 3b, 3d, and 10a) indicate that the gravity-driven
600 mass flow deposits (e.g., submarine landslides and debris flows) largely contributed to the TMF
601 formation by filling the sediment accommodation space in the middle to lower slope, where the
602 slope gradient is less than 1° (1100 to 1700 mwd: 0.9°; 1700 to 2200 mwd: 0.8°). This infilling
603 may have led to a gradual decrease of the overall slope gradient (e.g., Faleide et al., 1996;
604 O'Grady & Syvitski, 2002), which enabled the accumulation of glaciogenic debris lobes on the
605 gentler slope of the southwestern Chukchi Rise margin. In contrast, a relatively high upper slope
606 gradient (>4°) of the northwestern Chukchi Rise margin could be a reason for the poorly

607 developed TMF (e.g., Batchelor & Dowdeswell, 2014; Ó Cofaigh et al., 2003; O’Grady &
608 Syvitski, 2002; Piper & Normark, 2009).

609 Sediment supply for the TMF formation is also controlled by the subglacial geology of
610 the continental shelf (Batchelor & Dowdeswell, 2014; Halberstadt et al., 2016; Ó Cofaigh et al.,
611 2003, 2004; Solheim et al., 1998; Winsborrow et al., 2010). Prior deep seismostratigraphic data
612 (Figure 1b) show that the pre-glacial strata with laterally continuous internal reflections are
613 widely developed and completely cover high-standing crustal blocks of the Chukchi Rise (Dove
614 et al., 2014; Hegewald & Jokat, 2013; Ilhan & Coakley, 2018). Weakly compacted marine
615 sediment can be much easier eroded by grounded ice rather than crystalline rock or glaciogenic
616 diamicton (e.g., Halberstadt et al., 2016; Moore, 1964; Ó Cofaigh et al., 2003; Wellner et al.,
617 2001; Winsborrow et al., 2010). With respect to TMF development, the seaward-dipping
618 bathymetric trough on the southwestern Chukchi Rise margin (Figure 1b) is relatively less
619 developed than landward-dipping glacial troughs (Batchelor & Dowdeswell, 2014). A seaward-
620 dipping trough can be easily eroded by repeated glacial advances despite a relatively short glacial
621 history, as exemplified by the Mackenzie Trough at the Canadian Arctic margin (Batchelor et al.,
622 2013). We infer that large quantities of sediment on the wide outer shelf of the southwestern
623 Chukchi Rise margin were eroded by the fast-flowing grounded ice and remobilized downslope.
624 This inference is consistent with the occurrence of large-scale glacial sediment T4/T3
625 depocenters on the mid-lower slope (Figures 4 and 10a).

626 Suspension settling from turbid meltwater plumes released from an ice-stream front can
627 also contribute to the TMF growth and form gullies on the slope (Gales et al., 2013; Ó Cofaigh et
628 al., 2003; Shipp et al., 1999). The development of gullies varies depending on the upper slope
629 gradient (Klages et al., 2015; Ó Cofaigh et al., 2003). Gullies are weakly developed on the gentle
630 (2 to 3°) southwestern slope of the Chukchi Rise, whereas deeply incised gullies occur on the
631 steep (>4°) northwestern slope (Figures 9a and 10b). This distribution implies that the TMF at
632 the southwestern Chukchi Rise margin has been formed by complex sedimentary processes
633 including debris flows and turbid meltwater plumes. Sedimentary deposits from turbid meltwater
634 are characterized by acoustically stratified facies (Joe et al., 2020; Taylor et al., 2002), such as
635 observed in our data between the debris flow packages (e.g., between T3b and T3a in Figure 4).

636 5.2.2 *Glaciogenic facies*

637 Based on the mapped distribution of glaciogenic deposits, major contributions to the
638 TMF at the southwestern Chukchi Rise margin can be attributed to the glacially-fed debris flows
639 of subunits T4/T3 and suspension settling from turbid meltwater plumes forming intercalated
640 stratified facies (Figures 2 to 5). Contributions of T2 are much smaller, although the T2
641 grounding zone wedge developed on the upper slope and outer shelf, while evidence from older
642 glaciations has not been preserved (Figures 3f and 6). This distribution indicates that the ice
643 sheet that formed T2 had the same or even larger extent than the previous glaciations in this area
644 so that changes in the glaciogenic inputs to the TMF had other controls. In general, the basal
645 thermal condition of an ice-sheet is a major control for sediment transport within a glacial system
646 (Frederick et al., 2016; MacGregor et al., 2016; Menzies & Shilts, 2002). Larger quantities of
647 sediment can be transported under temperate, wet than under cold polar/subpolar basal
648 conditions (Alley et al., 1997; Benn & Evans, 2014; Davis et al., 2006; Kirkbride, 2002; Ottesen
649 et al., 2005; Schomacker et al., 2010; Vorren & Laberg, 1997). In addition, proglacial
650 sedimentation is strongly affected by the volume of meltwater and its proximity to the ice margin

651 (C. H. Eyles & Eyles, 2010; Menzies & van der Meer, 2018). As a result, faster-flowing ice-
652 sheets with wet-based basal conditions could support more extensive sediment transportation and
653 deposition at larger water depths. Another factor is that during the formation of T4/T3, large
654 volumes of sediments were probably accumulated at the shelf break by subglacial transport of
655 the readily erodible pre-glacial or ice-distal sediments, and subsequently remobilized downslope.
656 In comparison, by the time of the T2 formation, most of the sediment on the outer shelf and
657 upper slope may have been already consumed by the downslope transport. Furthermore, the
658 older strata exposed on the shelf possibly became more compacted by ice-sheet loading (e.g.,
659 Böhm et al., 2009).

660 The continental slope of the western spur and the northwestern Chukchi Rise margin is
661 mainly covered by well-developed stratified sediment layers (S4 to S1) with insignificant lateral
662 variation (Figures 3a, 3c, 3e, and 3g), except for the T1 accumulation at the northwestern outer
663 shelf (Figures 3h and 7). This pattern indicates that gravity-driven mass flow processes were less
664 active here than at the southwestern margin, probably due to colder basal conditions and/or lower
665 sediment fluxes at a more northern location further away from the continental margin. The
666 delivery of sediment to the western spur and the northwestern slope likely occurred mainly by
667 iceberg-rafting and hemipelagic sedimentation, as common for proglacial glaciomarine
668 environments (Ó Cofaigh et al., 2003). The stratified deposits of S4 (or S3 at some sites) to S1 in
669 this area drape the pre-glacial slope features, such as sediment waves and gullies (Figures 8f, 8g,
670 and 9a). This stratigraphy indicates that the active marine down- and along-slope sedimentary
671 processes were diminished since the onset of glaciations when depositional environments
672 became predominantly glaciomarine.

673 The location of the major T1 glaciogenic depocenter on the outer shelf at relatively
674 shallow water depths of <450 m (Figures 3h and 10a), suggests that T1 was deposited by a
675 smaller and younger ice sheet than T2. Seismostratigraphic correlation of the boundary between
676 U1 and U2 (Figure 2) further indicates that the formation of T1 postdated T2. This evidence is
677 consistent with a lower thickness of acoustically stratified sediment on top of T1 at the
678 northwestern margin (<1 m) than on T2 further south (>5 m) (Figures 3g, 6, and 7), resulting in
679 well-expressed channels on top of T1 (Figures 7c and 10a). In comparison, the T2 surface
680 features a hummocky proglacial moraine and well-developed gas seepage mounds indicative of a
681 stronger glacial impact and/or longer post-glacial period. We note, however, that the thickness of
682 post-glacial sediments depends not only on the time of deposition but also on sediment
683 dynamics. It has been shown for the study region that sedimentation rates since the last major
684 glaciation overall decrease northwards indicating sediment sources further south (Schreck et al.,
685 2018).

686

687 5.3 Past ice-sheet dynamics and related processes

688 The fast-flowing ice streams marked in suitable seafloor sediments by the MSGL are
689 primarily constrained by the ice sheet's mass balance, subglacial topography, and geology (e.g.,
690 Halberstadt et al., 2016). In general, the preserved MSGL indicates the latest grounded ice flow
691 just before a final ice retreat, typically by floatation and breakup (e.g., Dowdeswell et al., 2008).
692 The combined MBES and SBP data from the Chukchi Rise indicate that the deeper located (780
693 to 940 mwd), SSW–NNE oriented MSGL on the middle slope of the western spur were formed
694 prior to the U2 deposits (Figures 8e and 9a). In comparison, N–S oriented MSGL overriding T2

695 on the outer shelf were clearly formed by a younger and thinner ice mass (Figures 8d and 9a).
696 This interpretation is consistent with the accumulation of acoustically stratified sediments with
697 low backscatter intensity on top of the deeper MSGL, but only a thin sediment cover with higher
698 backscatter intensity on top of the outer shelf MSGL (Figures 8d, 8e, and 9a).

699 Both MSGL sets occur on a relatively elevated topography, with their general orientation
700 subparallel to the local shelf edge (Figures 9a and 10b), unlike typical MSGL in the cross-shelf
701 glacial troughs (e.g., Batchelor & Dowdeswell, 2014; Dowdeswell et al., 2008; Halberstadt et al.,
702 2016; Shipp et al., 1999). In addition to the lack of a pronounced topographic depression, the
703 distribution of T4 and T3 deposits does not indicate any grounded ice in the MSGL area. This
704 pattern suggests that the MSGL were probably formed by a relatively short-lived, passing ice
705 flow from a thicker ice sheet, potentially formed on the continental margin. The episodic nature
706 of such an ice flow may have been beneficial for MSGL preservation. There is also a possibility
707 that these MSGL could be “plane furrows” produced by huge, tilted tabular icebergs derived
708 from a collapsing ice shelf (Dowdeswell & Bamber, 2007; Wellner et al., 2006). Such furrows
709 are relatively sparse in comparison with the MSGL fields but extend longer with high linearity
710 than typical iceberg plowmarks observed on the Chukchi margin at water depths shallower than
711 ~350 m (Dove et al., 2014) (Figure 9). We note that MSGL and “plane furrows” may co-occur in
712 areas of the past ice-flow/ice-shelf break-up (Wellner et al., 2006).

713 The sets of laterally extended, isobath-parallel recessional moraines on the outer shelf to
714 upper slope of the western margin are apparently associated mostly with the T2 deposits (Figures
715 8d and 9a). A prominent stand-alone ridge at shallower water depths of ~400–420 m might
716 indicate a younger glacial event (Figure 9a). This ridge overrides the MSGL in this area and thus
717 was formed after the ice streaming event marked by the MSGL. Overall the ridges likely indicate
718 a stepwise up-slope retreat of the ice-sheet grounding line controlled by the rising sea levels
719 during deglaciation(s) (Batchelor et al., 2018; Jakobsson et al., 2008; Ottesen & Dowdeswell,
720 2006; Polyak et al., 2001). This pattern contrasts with the bathymetry independent MSGL
721 controlled by the ice-sheet mass balance and topography during ice-sheet collapsing events. The
722 ice-sheet collapses and retreats on the Chukchi Rise may have been triggered by the instability of
723 an ice shelf (shelves) over the adjacent basins in the absence of pinning points (e.g., Halberstadt
724 et al., 2016; Jakobsson et al., 2016; Wellner et al., 2001). Different patterns of the recessional
725 ridge fields on the western spur and the southwestern margin may reflect a lateral variability in
726 the retreat rapidity (Figures 9a and 10b). The western spur features multiple recessional ridges
727 with a high lateral continuity, indicating a relatively gradual, stepwise retreat (e.g., Dowdeswell
728 et al., 2008) (Figures 9a and 10b). The sparser, less developed recessional moraines on the outer-
729 shelf terrace of the southwestern margin possibly indicate a more abrupt retreat of the grounding
730 line from the shelf edge to the inner shelf (Figures 6, 9a, and 10b). The faster retreat may have
731 been facilitated by a deeper shelf break and a flatter gradient of the shelf-edge terrace in the
732 southwestern area (Figures 9a and 10b).

733 The area of hummocky moraines and mounds developed on the southwestern outer shelf
734 and upper slope is covered by a moderately thick acoustically stratified sediment of S1 with
735 relatively low backscatter intensity (Figures 8b and 9a). This pattern indicates a farther/earlier
736 shelfward retreat of the grounded ice sheet in this area than further north on the western spur and
737 the northwestern margin featuring thinner overlying stratified sediments and higher backscatter
738 intensity (Figures 9a and 10b). The seepage-related mound structures preserved on the outer
739 shelf and upper slope of the southwestern margin also pre-date the U1 deposits (Kim et al., 2020)

740 (Figure 8b), thus indicating no ice-sheet re-advance in this area after the T2 formation (Figure
741 10b).

742 Based on the stratigraphic position of the buried incised surface and the thickness of the
743 overlying acoustically stratified sediments, the gullies on the northwestern slope (Figures 8f and
744 9a) are probably older (pre-U3) than at the southwestern margin (U2; Figures 8a and 9a). The
745 gully formation can be explained by a grounded ice advance to the shelf edge that provided
746 turbid meltwater pulses capable of incising canyons on the steep slope (Lowe & Anderson, 2003;
747 Ó Cofaigh et al., 2003). After the gully formation event at the northwestern slope, no sufficient
748 sediment-laden meltwater was generated in this area, possibly due to a change in the basal
749 thermal condition from the temperate-wet to the polar-cold (Rebesco & Camerlenghi, 2008). The
750 younger and smaller gullies on the southwestern slope indicate overall lower amounts of
751 subglacial meltwater discharged during the T2 glacial event. In comparison to the deeper located
752 slope gullies, the fresh-looking, relatively shallow but broad (up to 1000 m) channels on top of
753 the T1 wedge on the northwestern shelf likely have a different nature. Considering their
754 geometry and the position on a gently dipping surface of the youngest glacial deposit, they may
755 be related to the subglacial drainage at the final deglacial stages. On the other hand, low
756 backscatter intensities of the T1 wedge surface (Figure 7c) are more common for proglacial
757 rather than subglacial deposits. Clarifying the nature of this glaciogenic accumulation requires
758 denser data coverage, including shelf-to-slope lines. Buried valleys reaching considerably larger
759 dimensions are widely distributed across the Chukchi margin (Dove et al., 2014; Hill et al., 2007;
760 Hill & Driscoll, 2008). Their common occurrence on the Chukchi Rise at water depths of >300
761 m indicates their subglacial rather than river-born origin (Dove et al., 2014).

762 The pre-glacial sediment waves expressed in bathymetry-parallel, undulating morphology
763 are well preserved on the slope of the western spur and the northwestern margin due to the
764 conformable geometry of the overlying acoustically stratified deposits of S4–S1 (Figure 8g). The
765 absence of similar undulations on the southwestern slope (Figure 9a) can be explained by the
766 burial of pre-glacial sediment waves by the thick TMF deposits (Dove et al., 2014; Hegewald &
767 Jokat, 2013; Ilhan & Coakley, 2018).

768

769 5.4 Glaciation history

770 5.4.1 Ice-sheet distribution and provenance

771 The overall distribution of glaciogenic seafloor morphology and sediment stratigraphy in
772 the study area is consistent with the notion that Arctic ice sheets advanced from the continental
773 margins toward the central Arctic Ocean and retreated upslope back to the margins and shallow
774 bathymetric areas (Dove et al., 2014; Engels et al., 2008; Jakobsson et al., 2008, 2010, 2014;
775 Polyak et al., 2001, 2007). If the entire Arctic Ocean was covered by a thick ice shelf during
776 some of the peak glaciations, it likely behaved as a single large ice mass outflowing into the
777 North Atlantic (Hughes et al., 1977; Jakobsson et al., 2016). Due to these changes in ice flow and
778 a lack of major topographic constraints, such as cross-shelf troughs or inter-island channels, the
779 directions of ice advances and retreats at the western Chukchi Rise margin are more complex
780 than on the well-developed glaciated margins around the Antarctic, Polar North Atlantic, and the
781 Canadian Arctic Archipelago (Batchelor et al., 2014; Batchelor & Dowdeswell, 2014;
782 Halberstadt et al., 2016; Ó Cofaigh et al., 2003; Winsborrow et al., 2010).

783 Prior MBES data from the Chukchi Borderland collected mostly east of the study area
784 indicate a prevalent SE–NW to ESE–WNW trending impact of grounded ice mass(es) projected
785 to originate from the northwestern sector of the Laurentide Ice Sheet (Figure 1a) (Dove et al.,
786 2014; Engels et al., 2008; Jakobsson et al., 2008, 2014; Polyak et al., 2001, 2007). Another
787 distinct set of directional seafloor features on the eastern side of the Chukchi Rise appears to
788 irradiate from the Chukchi Shelf (Dove et al., 2014; Jakobsson et al., 2014), as also observed in
789 our ancillary data (Figure 9c). The co-occurrence of these major flowline trends makes a
790 complex picture reflecting the interaction of different ice flows. The evidence for ice provenance
791 in our seismostratigraphic and geomorphic data from the western side of the Chukchi Rise
792 provides another important piece for this puzzle picture.

793 Based on the TMF location in the seaward-dipping bathymetric trough at the
794 southwestern Chukchi Rise margin and the distribution of glaciogenic deposits T4/T3 preserved
795 on the slope, the general ice flow direction in this area was probably northwestward from the
796 Chukchi Shelf toward the Chukchi Basin (Figure 10a). A similar, more S–N orientation of an
797 MSGL set on the outer shelf formed apparently on top of T2 (Figure 9a) also suggests an ice
798 flow from the Chukchi margin. The prominent grounding zone till wedges on the western margin
799 at the shelf edge and further shelfward probably mark standstill positions of the grounded ice
800 margins (Figure 10b). The up-slope deglacial retreat of the ice margins is marked by sets of
801 recessional moraines (Figure 8d, 9a, and 10b), also observed at the northern Chukchi Rise tip
802 (Figure 9b) and in prior data from the Chukchi Rise and Cap further east and north (Dove et al.,
803 2014; Jakobsson et al., 2008). In our data, these ridges appear to be primarily associated with T2.
804 Similar grounding zone standstill and retreat features for T4/T3 apparently have not been
805 preserved.

806 The overall picture emerging from these data indicates that ice coming from the
807 Laurentide Ice Sheet may have been deflected northwards (i.e., towards the Canada Basin) by the
808 ice sheet(s) irradiating from the Chukchi margin. Alternatively, it can also be inferred that the
809 younger Chukchi-centered ice sheets overprinted the depositional/geomorphic evidence of the
810 older ice masses with different flow trajectories. Considering that our data cover four glacial
811 intervals with a long glacial history, it is more likely that coeval ice masses with different
812 provenance actually interacted on the Chukchi Rise. We note that while multiple seafloor
813 features indicate ice flow(s) from the Chukchi continental margin, they cannot be confirmed by
814 data from the shelf itself (Dove et al., 2014; Jakobsson et al., 2014). The obvious reason for this
815 lack of evidence is that sedimentary bedforms cannot preserve on the shallow, current-swept
816 Chukchi Shelf. Deeper geophysical records and drilling boreholes are needed to resolve this
817 gaping blind spot.

818 On the western side of the Chukchi Rise, the ice-flow interactions can also be envisaged
819 with the East Siberian Ice Sheet. While still sketchily understood, this ice sheet is corroborated
820 by multiple seafloor data (Jakobsson et al., 2016; Joe et al., 2020; Niessen et al., 2013; O'Regan
821 et al., 2017; Schreck et al., 2018) and paleoclimatic modeling studies (Colleoni et al., 2016;
822 Gasson et al., 2018). If the ice shelves extending from the East Siberian and Chukchi margins
823 consequently coalesced and started to behave like a single large ice mass (Hughes et al., 1977;
824 Jakobsson et al., 2016), the flow direction would have been re-oriented towards the central
825 Arctic Ocean, orthogonally to the Chukchi–East Siberian margin. This orientation may have
826 accounted for the SSW–NNE trending, deep-sited MSGL on top of the T3 deposits on the
827 western spur (Figure 10b). The large water depth of these features (>900 m) is similar to the ice

828 grounding on the Lomonosov Ridge in the center of the Arctic Ocean (Jakobsson et al., 2001,
829 2008, 2010, 2014; Polyak et al., 2001). Elaborating these mechanisms is important for
830 understanding the behavior of the Arctic glaciations and, more generally, the large marine-based
831 ice complexes.

832 5.4.2 Age framework

833 While there are no direct constraints for the age of the mapped glaciogenic deposits, a
834 tentative age framework can be outlined from stratigraphic data available from the adjacent areas
835 (Dipre et al., 2018; Joe et al., 2020; Polyak et al., 2007; Schreck et al., 2018; Wang et al., 2013).
836 In particular, combined geological/geophysical data from the southeastern part of the Chukchi
837 Borderland (ramp to the Northwind Ridge; Figure 1b) provide age constraints for the last two
838 glacial events impacting this seafloor area (Polyak et al., 2007). Glacial diamicton dated to the
839 Last Glacial Maximum (LGM) of the Marine Isotope Stage (MIS) 2, ca. 15–25 ka, is associated
840 with the W–E trending MSGL at modern water depths to ~420–430 m. A nearby MSGL field
841 mapped at the southeastern side of the Chukchi Rise and presented in this study has similar
842 bathymetric and geomorphic characteristics (Figures 1b and 9c). The MSGL orientations in these
843 two fields indicate ice streaming from the Chukchi margin. This picture is consistent with the
844 distribution of the T1 deposits at the western Chukchi Rise, which is restricted to water depths of
845 <450 m and are covered with only thin post-glacial sediments (Figures 3h, 7, and 10a). Well-
846 expressed channels on top of the T1 deposit at the northwestern shelf possibly represent the pro-
847 or subglacial drainage during deglaciation, similar to, but younger than buried valleys reported
848 for the Chukchi Rise by Dove et al. (2014). These characteristics of the T1 deposits allow for
849 attribution of their formation to the LGM. This interpretation is also consistent with sediment-
850 core evidence from the Chukchi Basin that suggests the presence of the LGM grounded ice
851 masses at shallower depths in this region (Joe et al., 2020; Schreck et al., 2018; Wang et al.,
852 2013).

853 Glacial deposits attributed to MIS 4 (ca. 60–70 ka) appear to be widely distributed in the
854 study region, including tills on the bathymetric highs, debris lobes on the slopes, and thick
855 glaciomarine deposits in the basins (Joe et al., 2020; Polyak et al., 2007; Schreck et al., 2018;
856 Wang et al., 2013). The corresponding glaciogenic bedforms such as MSGL and morainic ridges
857 extend to the shelf edge at ~600–700 mwd (Dove et al., 2014; Jakobsson et al., 2008; Polyak et
858 al., 2007). At the southern Northwind Ridge, these deposits feature the SE–NW trending MSGL
859 indicative of an ice flow from the Laurentide Ice Sheet (Polyak et al., 2007). MSGL with a
860 similar orientation and depth range are also widely reported elsewhere from the Northwind
861 Ridge, Chukchi Cap, and Alaskan margin (Dove et al., 2014; Engels et al., 2008; Jakobsson et
862 al., 2005, 2008). The seismostratigraphic and bathymetric position of the T2 deposits indicates
863 their probable relation to the co-eval glacial event. The seismostratigraphic boundaries of U2,
864 including T2 (H2/H3, Figure 2a), apparently correspond to reflectors R2/R3 defined for the East
865 Siberian (Arliss Plateau) slope across the Chukchi Basin (Joe et al., 2020). These reflectors were
866 related to prominent IRD layers formed by the iceberg discharge pulses from the Laurentide Ice
867 Sheet during the deglaciations following and preceding MIS 4. Despite probable synchronicity
868 with a Laurentide-sourced ice advance inferred for more eastern areas, this glaciation on the
869 western Chukchi Rise apparently had a different provenance based on the S–N-trending
870 orientation of the MSGL on top of T2. According to this orientation, the main grounded ice was
871 located south of the Chukchi Rise at least at the late glacial stages. This inference is consistent
872 with the formation of a hummocky moraine south of the MSGL field (Figure 9a).

873 The age controls for the older glacial deposits T4/T3 preserved in the study area only as
874 debris lobes on the slope are more speculative. The potentially largest glacial impact in the
875 Arctic has been inferred for MIS 6 (late Middle Pleistocene, ca. 130–190 ka) based on a very
876 deep (>1 km) ice grounding on the Lomonosov Ridge in the center of the Arctic Ocean
877 constrained to this glacial interval (Jakobsson et al., 2001, 2010, 2014, 2016; Polyak et al.,
878 2001). Reconstructed circum-Arctic ice-sheet limits also show a very large extent for the
879 northern North America and the largest for the northern Eurasia (Batchelor et al., 2019 and
880 references therein). Glacial diamicton probably of this age has been recovered on top of the
881 northern part of the Northwind Ridge in front of a prominent morainic ridge (Dipre et al., 2018;
882 Jakobsson et al., 2010). A large pre-MIS 4 debris lobe on the East Siberian slope (Arliss Plateau:
883 Joe et al., 2020) may also belong to the MIS 6. A possible attribution of the glaciogenic T3
884 deposits to this glaciation is indirectly supported by the MSGL set formed at water depths to
885 >900 m on top of T3 and aligned with the direction towards the central Arctic Ocean (Figures 9a
886 and 10). Two glaciogenic lobes identified as subunits of T3 (Figure 4) indicate two glacial
887 events, possibly stages of the same glaciation.

888 The age of the oldest glaciogenic unit T4 can be considered in relation to the history of a
889 large-scale glacial erosion on the Chukchi margin/borderland. Based on regional airgun seismic
890 data, the glaciogenic erosional boundary occurs on top of deposits overlying the late Miocene
891 unconformity and is broadly attributed to Plio-Pleistocene (Hegewald, 2012; Hegewald & Jokat,
892 2013; Ilhan & Coakley, 2018). In sediment cores from the northern Northwind Ridge the contact
893 between pre-glacial and glaciogenic strata is constrained by cyclostratigraphy and strontium
894 isotope dating to MIS 16/20, ca. 0.7–0.9 Ma (Dipre et al., 2018; Polyak et al., 2013). This timing
895 corresponds to a prominent change in paleoclimatic conditions (Mid-Pleistocene Transition)
896 related to a shift in the prevailing orbital cyclicities and the development of huge ice sheets in the
897 Northern Hemisphere in the Middle Pleistocene starting with MIS 16 (Clark et al., 2006; Lisiecki
898 & Raymo, 2005).

899 Based on the airgun seismic data, there is one glaciogenic sedimentary package between
900 the reflector H5 (lower boundary of unit U4) and the initial glaciogenic unconformity (Dove et
901 al., 2014) (H6; Figure S3). This stratigraphy indicates that T4 was formed during the second
902 regional glacial event. If the first glacial expansion occurred in MIS 16 or somewhat earlier, the
903 T4 age can be placed somewhere in the lower part of the Middle Pleistocene, such as MIS 12
904 that was a prominent glaciation based on a sedimentary record from the Canada Basin (Dong et
905 al., 2017).

906 Constraining the outlined stratigraphic estimates more conclusively requires more
907 sediment cores, preferably with long records such as pursued by the International Ocean
908 Discovery Program (IODP). Our data may contribute useful information for developing an IODP
909 project in the Chukchi region.

910

911 **6 Summary and conclusions**

912 This study presents the detailed, high-resolution sub-bottom profiler (SBP) and
913 multibeam echosounder (MBES) data from the Chukchi Rise in the western Arctic Ocean. The
914 combined seismostratigraphic and morphobathymetric analysis sheds new light on the past ice-
915 sheet/ice-shelf distribution and dynamics and related sedimentary/geomorphic processes. Results

916 of this study provide important empirical constraints for reconstructing Quaternary glaciations in
917 and around the Arctic Ocean.

918 Based on the acoustic character of sediments revealed by the SBP data, we identify four
919 seismostratigraphic units, U4–U1, each including acoustically stratified and transparent facies
920 classified as subunits S4–S1 and T4–T1, respectively. The transparent facies are interpreted as
921 glaciogenic sediments deposited during glacial events probably spanning most of the Middle to
922 Late Pleistocene (ca. 0.5–1 Ma). The older transparent deposits (T4/T3) are preserved on the
923 southwestern mid-lower slope of the Chukchi Rise as debris lobes contributing to a large trough
924 mouth fan identified on the regional airgun seismic records. On the upper slope to outer shelf,
925 these features are replaced by a younger, wedge- to sheet-shaped deposit (T2) with an erosional
926 lower boundary and glaciogenic bedforms at the surface, such as mega-scale glacial lineations
927 (MSGSL), recessional morainic ridges, and hummocky moraines. The main T2 deposit at the shelf
928 break is interpreted as a glacial grounding zone wedge possibly formed during MIS 4 (ca. 60–70
929 ka). The youngest transparent deposit (T1), attributed to the Last Glacial Maximum (MIS 2, ca.
930 15–25 ka), occurs on the outer shelf at shallower water depths.

931 Two mapped sets of MSGSL trending SSW–NNE on top of T3 on the middle slope and S–
932 N on T2 on the outer shelf demonstrate at least two fast ice-streaming events of different ages.
933 The older, deeper sited (ca 780–940 mwd) MSGSL may be related to a passage of a large ice shelf
934 formed over the western Arctic Ocean. Contour-parallel, nested recessional-moraine ridges are
935 identified along the outer shelf to upper slope on top of the grounding zone deposits. Correlative
936 ridges are also mapped north of the main study area, thus indicating their distribution along the
937 entire Chukchi Rise margin. The well-developed ridges mark a stepwise retreat of the grounded
938 ice margin, likely controlled by rising sea levels during deglaciation(s). More random ridges at a
939 flatter bathymetric bench on the southwestern margin may indicate a faster retreat. The different
940 orientations of ice advances and retreats reflect a complex geomorphic setting of the borderland
941 that lacks major topographic controls typical for glaciated continental margins, such as cross-
942 shelf glacial troughs.

943 The seismostratigraphic and geomorphic data suggest that ice flow directions for all of
944 the identified glacial events were principally from the Chukchi continental margin south of the
945 study area. Based on the additional mapping and prior data, the same ice-sheet origin can be
946 projected for glaciogenic bedforms on the eastern side of the Chukchi Rise, along with the
947 evidence of ice flow(s) apparently originating from the northwestern Laurentide Ice Sheet. This
948 complex picture shows that the Chukchi Rise was an area of intense interaction(s) of different
949 ice-sheets/ice-shelves that affected the overall glaciation development in the Arctic Ocean.

950 In addition to glaciogenic deposits and bedforms, our data identify a number of related or
951 independent seabed features including mounds, gullies/channels, and sediment waves. Mounds,
952 presumably formed by gas seepage, grow from the surface of the T2 deposit, possibly triggered
953 by glaciogenic pressure effects. Buried gullies on the upper slope were likely incised by
954 proglacial turbid water flows, while fresh-looking, broad channels on top of the T1 deposit on
955 the shelf may be related to the pro- or subglacial drainage during the last deglaciation. Sediment
956 waves are characteristic for pre-glacial sediments on the middle slope, thus indicating active
957 hydrodynamic conditions at the intermediate water depths before the onset of major glaciations.

958

959 **Acknowledgments**

960 The authors are grateful to the captain and crew of the IBRV *Araon* for their help
 961 provided during the Arctic expeditions since 2012. This work was supported by the Korea Polar
 962 Research Institute (KOPRI) Grant PM20050 (KIMST Grant 20160247). Y. J. Joe and S.-I. Nam
 963 acknowledge funding from the KOPRI Grant PE20350. F. Niessen was funded by the AWI
 964 Research Program PACES-II, Workpackages 3.1 and 3.2. We thank SeisWare Inc. for the
 965 academic grant program for using the software for seismostratigraphic analysis and mapping.
 966 SBP data processing, MBES data gridding, and mapping were conducted using the open-source
 967 software Seismic Unix (<https://wiki.seismic-unix.org>), Generic Mapping Tools
 968 (<https://www.generic-mapping-tools.org>), and QGIS (<https://qgis.org>). The MBES
 969 bathymetry/backscatter and units/subunits thickness mapping results used in this study are
 970 archived by the Korea Polar Data Center and are available at <https://kpdc.kopri.re.kr>.

971 **Appendix A. Supplementary data**

972 Supplementary data to this article can be found online at
 973 “<https://dx.doi.org/doi:10.22663/KOPRI-KPDC-00001625.1>”.

974

975 **References**

- 976 Alley, R. B., Blankenship, D. D., Bentley, C. R., & Rooney, S. T. (1986). Deformation of till
 977 beneath ice stream B, West Antarctica. *Nature*, (6074), 57–59.
- 978 Alley, R. B., Cuffey, K., Evenson, E., Strasser, J., Lawson, D., & Larson, G. (1997). How
 979 glaciers entrain and transport basal sediment: physical constraints. *Quaternary Science*
 980 *Reviews*, 16(9), 1017–1038. [https://doi.org/10.1016/S0277-3791\(97\)00034-6](https://doi.org/10.1016/S0277-3791(97)00034-6)
- 981 Anderson, J. B. (1999). *Antarctic marine geology* (Vol. 289). Cambridge Univ Press.
- 982 Batchelor, C. L., & Dowdeswell, J. A. (2014). The physiography of High Arctic cross-shelf
 983 troughs. *Quaternary Science Reviews*, 92, 68–96.
 984 <http://dx.doi.org/10.1016/j.quascirev.2013.05.025>
- 985 Batchelor, C. L., Dowdeswell, J. A., & Pietras, J. T. (2013). Seismic stratigraphy, sedimentary
 986 architecture and palaeo-glaciology of the Mackenzie Trough: evidence for two
 987 Quaternary ice advances and limited fan development on the western Canadian Beaufort
 988 Sea margin. *Quaternary Science Reviews*, 65, 73–87.
 989 <http://dx.doi.org/10.1016/j.quascirev.2013.01.021>
- 990 Batchelor, C. L., Dowdeswell, J. A., & Pietras, J. T. (2014). Evidence for multiple Quaternary
 991 ice advances and fan development from the Amundsen Gulf cross-shelf trough and slope,
 992 Canadian Beaufort Sea margin. *Marine and Petroleum Geology*, 52, 125–143.
 993 <http://dx.doi.org/10.1016/j.marpetgeo.2013.11.005>
- 994 Batchelor, C. L., Ottesen, D., & Dowdeswell, J. A. (2017). Quaternary evolution of the northern
 995 North Sea margin through glacial debris-flow and contourite deposition. *Journal of*
 996 *Quaternary Science*, 32(3), 416–426. <https://doi.org/10.1002/jqs.2934>

- 997 Batchelor, C. L., Dowdeswell, J. A., & Ottesen, D. (2018). Submarine Glacial Landforms. In A.
 998 Micallef, S. Krastel, & A. Savini (Eds.), *Submarine Geomorphology* (pp. 207–234).
 999 Cham: Springer International Publishing. https://doi.org/10.1007/978-3-319-57852-1_12
- 1000 Batchelor, C. L., Margold, M., Krapp, M., Murton, D. K., Dalton, A. S., Gibbard, P. L., et al.
 1001 (2019). The configuration of Northern Hemisphere ice sheets through the Quaternary.
 1002 *Nature Communications*, *10*(1), 3713. <https://doi.org/10.1038/s41467-019-11601-2>
- 1003 Benn, D., & Evans, D. J. (2014). *Glaciers and glaciation* (Second). Hodder Education.
- 1004 Bennett, M. R., Huddart, D., Hambrey, M. J., & Ghienne, J. F. (1996). Moraine Development at
 1005 the High-Arctic Valley Glacier Pedersenbreen, Svalbard. *Geografiska Annaler: Series A,*
 1006 *Physical Geography*, *78*(4), 209–222. <https://doi.org/10.1080/04353676.1996.11880468>
- 1007 Böhm, G., Ocakoğlu, N., Picotti, S., & De Santis, L. (2009). West Antarctic Ice Sheet evolution:
 1008 New insights from a seismic tomographic 3D depth model in the Eastern Ross Sea
 1009 (Antarctica). *Marine Geology*, *266*(1), 109–128.
- 1010 Boone, S. J., & Eyles, N. (2001). Geotechnical model for great plains hummocky moraine
 1011 formed by till deformation below stagnant ice. *Geomorphology*, *38*(1), 109–124.
 1012 [https://doi.org/10.1016/S0169-555X\(00\)00072-6](https://doi.org/10.1016/S0169-555X(00)00072-6)
- 1013 Bradwell, T., Stoker, M. S., Golledge, N. R., Wilson, C. K., Merritt, J. W., Long, D., et al.
 1014 (2008). The northern sector of the last British Ice Sheet: Maximum extent and demise.
 1015 *Earth-Science Reviews*, *88*(3), 207–226. <https://doi.org/10.1016/j.earscirev.2008.01.008>
- 1016 Clark, P. U., Archer, D., Pollard, D., Blum, J. D., Rial, J. A., Brovkin, V., et al. (2006). The
 1017 middle Pleistocene transition: characteristics, mechanisms, and implications for long-
 1018 term changes in atmospheric pCO₂. *Quaternary Science Reviews*, *25*(23), 3150–3184.
 1019 <https://doi.org/10.1016/j.quascirev.2006.07.008>
- 1020 Coakley, B. J., Ilhan, I., & Chukchi Edges Science Party. (2011). Chukchi Edges Project-
 1021 Geophysical constraints on the history of the Amerasia Basin. In *AGU Fall Meeting*
 1022 *Abstracts* (Vol. 1, p. 2365).
- 1023 Colleoni, F., Kirchner, N., Niessen, F., Quiquet, A., & Liakka, J. (2016). An East Siberian ice
 1024 shelf during the Late Pleistocene glaciations: Numerical reconstructions. *Quaternary*
 1025 *Science Reviews*, *147*(Special Issue: PAST Gateways (Palaeo-Arctic Spatial and
 1026 Temporal Gateways)), 148–163.
- 1027 Darby, D. A., Jakobsson, M., & Polyak, L. (2005). Icebreaker expedition collects key Arctic
 1028 seafloor and ice data. *Eos, Transactions American Geophysical Union*, *86*(52), 549–552.
- 1029 Davis, P. T., Briner, J. P., Coulthard, R. D., Finkel, R. W., & Miller, G. H. (2006). Preservation
 1030 of Arctic landscapes overridden by cold-based ice sheets. *Quaternary Research*, *65*(1),
 1031 156–163. <https://doi.org/10.1016/j.yqres.2005.08.019>
- 1032 DeConto, R. M., & Pollard, D. (2016). Contribution of Antarctica to past and future sea-level
 1033 rise. *Nature*, *531*(7596), 591–597.
- 1034 Dipre, G. R., Polyak, L., Kuznetsov, A. B., Oti, E. A., Ortiz, J. D., Brachfeld, S. A., et al. (2018).
 1035 Plio-Pleistocene sedimentary record from the Northwind Ridge: new insights into
 1036 paleoclimatic evolution of the western Arctic Ocean for the last 5 Ma. *Arktos*, (1), 24.

- 1037 Donda, F., O'Brien, P., De Santis, L., Rebesco, M., & Brancolini, G. (2008). Mass wasting
 1038 processes in the Western Wilkes Land margin: possible implications for East Antarctic
 1039 glacial history. *Palaeogeography, Palaeoclimatology, Palaeoecology*, *260*(1), 77–91.
- 1040 Dong, L., Liu, Y., Shi, X., Polyak, L., Huang, Y., Fang, X., et al. (2017). Sedimentary record
 1041 from the Canada Basin, Arctic Ocean: implications for late to middle Pleistocene glacial
 1042 history. *Climate of the Past*, *13*(5), 511–531. <https://doi.org/10.5194/cp-13-511-2017>
- 1043 Dove, D., Polyak, L., & Coakley, B. J. (2014). Widespread, multi-source glacial erosion on the
 1044 Chukchi margin, Arctic Ocean. *Quaternary Science Reviews*, *92*, 112–122.
- 1045 Dowdeswell, J. A., & Bamber, J. L. (2007). Keel depths of modern Antarctic icebergs and
 1046 implications for sea-floor scouring in the geological record. *Marine Geology*, *243*(1),
 1047 120–131.
- 1048 Dowdeswell, J. A., & Siegert, M. J. (1999). Ice-sheet numerical modeling and marine
 1049 geophysical measurements of glacier-derived sedimentation on the Eurasian Arctic
 1050 continental margins. *Geological Society of America Bulletin*, *111*(7), 1080–1097.
- 1051 Dowdeswell, J. A., Kenyon, N., Elverhøi, A., Laberg, J., Hollender, F., Mienert, J., & Siegert, M.
 1052 (1996). Large-scale sedimentation on the glacier-influenced Polar North Atlantic
 1053 margins: long-range side-scan sonar evidence. *Geophysical Research Letters*, *23*(24),
 1054 3535–3538.
- 1055 Dowdeswell, J. A., Cofaigh, C. Ó., & Pudsey, C. J. (2004). Thickness and extent of the
 1056 subglacial till layer beneath an Antarctic paleo-ice stream. *Geology*, *32*(1), 13–16.
- 1057 Dowdeswell, J. A., Ottesen, D., Evans, J., Cofaigh, C. Ó., & Anderson, J. (2008). Submarine
 1058 glacial landforms and rates of ice-stream collapse. *Geology*, *36*(10), 819–822.
- 1059 Dowdeswell, J. A., Canals, M., Jakobsson, M., Todd, B. J., Dowdeswell, E. K., & Hogan, K. A.
 1060 (2016). *Atlas of Submarine Glacial Landforms: Modern, Quaternary and Ancient*. (J. A.
 1061 Dowdeswell, M. Canals, M. Jakobsson, B. J. Todd, E. K. Dowdeswell, & K. A. Hogan,
 1062 Eds.) (Vol. 46). Geological Society of London.
- 1063 Elvenes, S., & Dowdeswell, J. A. (2016). Possible “lift-off moraines” at grounded ice-sheet
 1064 margins, North Norwegian shelf edge. *Geological Society, London, Memoirs*, *46*(1), 247–
 1065 248.
- 1066 Elverhøi, A., Dowdeswell, J. A., Funder, S., Mangerud, J., & Stein, R. (1998). Glacial and
 1067 oceanic history of the Polar North Atlantic Margins: An Overview. *Quaternary Science*
 1068 *Reviews*, *17*(1), 1–10. [http://dx.doi.org/10.1016/S0277-3791\(97\)00073-5](http://dx.doi.org/10.1016/S0277-3791(97)00073-5)
- 1069 Engels, J. L., Edwards, M. H., Polyak, L., & Johnson, P. D. (2008). Seafloor evidence for ice
 1070 shelf flow across the Alaska–Beaufort margin of the Arctic Ocean. *Earth Surface*
 1071 *Processes and Landforms*, *33*(7), 1047–1063. <https://doi.org/10.1002/esp.1601>
- 1072 Eyles, C. H., & Eyles, N. (2010). Glacial deposits. In *Facies Models 4* (pp. 73–104). The
 1073 Geological Association of Canada’.
- 1074 Eyles, C. H., Eyles, N., & Lagoe, M. B. (1991). The Yakataga Formation: A six million year
 1075 record of temperate glacial marine sedimentation in the Gulf of Alaska. In J. B. Anderson
 1076 & G. M. Ashley (Eds.), *Glacial Marine Sedimentation: Paleoclimatic Significance* (Vol.
 1077 261, pp. 159–180). Geological Society of America.

- 1078 Eyles, N., Boyce, J. I., & Barendregt, R. W. (1999). Hummocky moraine: sedimentary record of
 1079 stagnant Laurentide Ice Sheet lobes resting on soft beds. *Sedimentary Geology*, *123*(3),
 1080 163–174. [https://doi.org/10.1016/S0037-0738\(98\)00129-8](https://doi.org/10.1016/S0037-0738(98)00129-8)
- 1081 Faleide, J. I., Solheim, A., Fiedler, A., Hjelstuen, B. O., Andersen, E. S., & Vanneste, K. (1996).
 1082 Late Cenozoic evolution of the western Barents Sea-Svalbard continental margin. *Global*
 1083 *and Planetary Change*, *12*(1), 53–74.
- 1084 Fransner, O., Noormets, R., Flink, A. E., Hogan, K. A., & Dowdeswell, J. A. (2017).
 1085 Sedimentary processes on the continental slope off Kvitøya and Albertini troughs north
 1086 of Nordaustlandet, Svalbard – The importance of structural-geological setting in trough-
 1087 mouth fan development. *Marine Geology*. <https://doi.org/10.1016/j.margeo.2017.10.008>
- 1088 Frederick, B. C., Young, D. A., Blankenship, D. D., Richter, T. G., Kempf, S. D., Ferraccioli, F.,
 1089 & Siegert, M. J. (2016). Distribution of subglacial sediments across the Wilkes
 1090 Subglacial Basin, East Antarctica. *Journal of Geophysical Research: Earth Surface*,
 1091 *121*(4), 790–813. <https://doi.org/10.1002/2015JF003760>
- 1092 Gales, J. A. (2013). *The geomorphology of Antarctic submarine slopes* (PhD Thesis). The
 1093 University of Manchester.
- 1094 Gales, J. A., Larter, R. D., Mitchell, N. C., & Dowdeswell, J. A. (2013). Geomorphic signature
 1095 of Antarctic submarine gullies: Implications for continental slope processes. *Marine*
 1096 *Geology*, *337*, 112–124.
- 1097 Gales, J. A., Larter, R. D., Leat, P. T., & Jokat, W. (2016). Components of an Antarctic trough-
 1098 mouth fan: examples from the Crary Fan, Weddell Sea. In Julian A Dowdeswell, M.
 1099 Canals, M. Jakobsson, B. J. Todd, E. K. Dowdeswell, & K. A. Hogan (Eds.), *Atlas of*
 1100 *Submarine Glacial Landforms: Modern, Quaternary and Ancient* (Vol. 46, pp. 377–378).
 1101 Geological Society, London, Memoirs.
- 1102 Gasson, E. G. W., DeConto, R. M., Pollard, D., & Clark, C. D. (2018). Numerical simulations of
 1103 a kilometre-thick Arctic ice shelf consistent with ice grounding observations. *Nature*
 1104 *Communications*, (1), 1510.
- 1105 Gulick, S. P. S., Shevenell, A. E., Montelli, A., Fernandez, R., Smith, C., Warny, S., et al.
 1106 (2017). Initiation and long-term instability of the East Antarctic Ice Sheet. *Nature*, *552*,
 1107 225–229.
- 1108 Halberstadt, A. R. W., Simkins, L. M., Greenwood, S. L., & Anderson, J. B. (2016). Past ice-
 1109 sheet behaviour: retreat scenarios and changing controls in the Ross Sea, Antarctica. *The*
 1110 *Cryosphere*, *10*(3), 1003–1020. <https://doi.org/10.5194/tc-10-1003-2016>
- 1111 Hall, J. K. (1990). Chukchi Borderland. In A. Grantz, L. Johnson, & J. F. Sweeney (Eds.), *The*
 1112 *Arctic Ocean Region* (Vol. L, pp. 337–350). The Geological Society of America.
- 1113 Hegewald, A. (2012). *The Chukchi Region-Arctic Ocean-Tectonic and Sedimentary Evolution*
 1114 (PhD Thesis). Chemistry and Geoscience University of Jena.
- 1115 Hegewald, A., & Jokat, W. (2013). Tectonic and sedimentary structures in the northern Chukchi
 1116 region, Arctic Ocean. *Journal of Geophysical Research: Solid Earth*, *118*(7), 3285–3296.
 1117 <http://dx.doi.org/10.1002/jgrb.50282>

- 1118 Hill, J. C., & Driscoll, N. W. (2008). Paleodrainage on the Chukchi shelf reveals sea level history
 1119 and meltwater discharge. *Marine Geology*, 254(3), 129–151.
 1120 <https://doi.org/10.1016/j.margeo.2008.05.018>
- 1121 Hill, J. C., Driscoll, N. W., Brigham-Grette, J., Donnelly, J. P., Gayes, P. T., & Keigwin, L.
 1122 (2007). New evidence for high discharge to the Chukchi shelf since the Last Glacial
 1123 Maximum. *Quaternary Research*, 68(2), 271–279.
- 1124 Himmler, T., Sahy, D., Martma, T., Bohrmann, G., Plaza-Faverola, A., Bünz, S., et al. (2019). A
 1125 160,000-year-old history of tectonically controlled methane seepage in the Arctic.
 1126 *Science Advances*, 5(8). <https://doi.org/10.1126/sciadv.aaw1450>
- 1127 Howat, I. M., Joughin, I., & Scambos, T. A. (2007). Rapid Changes in Ice Discharge from
 1128 Greenland Outlet Glaciers. *Science*, 315(5818), 1559–1561.
 1129 <https://doi.org/10.1126/science.1138478>
- 1130 Huang, Z., Siwabessy, J., Cheng, H., & Nichol, S. (2018). Using Multibeam Backscatter Data to
 1131 Investigate Sediment-Acoustic Relationships. *Journal of Geophysical Research: Oceans*,
 1132 123(7), 4649–4665. <https://doi.org/10.1029/2017JC013638>
- 1133 Hughes, T., Denton, G., & Grosswald, M. (1977). Was there a late-Würm Arctic ice sheet?
 1134 *Nature*, 266(5603), 5967602.
- 1135 Hunkins, K., Herron, T., Kutschale, H., & Peter, G. (1962). Geophysical studies of the Chukchi
 1136 Cap, Arctic Ocean. *Journal of Geophysical Research*, 67, 235–247.
- 1137 Ilhan, I., & Coakley, B. J. (2018). Meso-Cenozoic evolution of the southwestern Chukchi
 1138 Borderland, Arctic Ocean. *Marine and Petroleum Geology*, 95, 100–109.
 1139 <https://doi.org/10.1016/j.marpetgeo.2018.04.014>
- 1140 Ivanov, V. V., Shapiro, G. I., Huthnance, J. M., Aleynik, D. L., & Golovin, P. N. (2004).
 1141 Cascades of dense water around the world ocean. *Progress in Oceanography*, 60(1), 47–
 1142 98. <https://doi.org/10.1016/j.pocean.2003.12.002>
- 1143 Jakobsson, M. (1999). First high-resolution chirp sonar profiles from the central Arctic Ocean
 1144 reveal erosion of Lomonosov Ridge sediments. *Marine Geology*, 158(1), 111–123.
 1145 [https://doi.org/10.1016/S0025-3227\(98\)00186-8](https://doi.org/10.1016/S0025-3227(98)00186-8)
- 1146 Jakobsson, M., Løvlie, R., Arnold, E. M., Backman, J., Polyak, L., Knutsen, J.-O., & Musatov,
 1147 E. (2001). Pleistocene stratigraphy and paleoenvironmental variation from Lomonosov
 1148 Ridge sediments, central Arctic Ocean. *Global and Planetary Change*, 31(1), 1–22.
 1149 [https://doi.org/10.1016/S0921-8181\(01\)00110-2](https://doi.org/10.1016/S0921-8181(01)00110-2)
- 1150 Jakobsson, M., Gardner, J. V., Vogt, P. R., Mayer, L. A., Armstrong, A., Backman, J., et al.
 1151 (2005). Multibeam bathymetric and sediment profiler evidence for ice grounding on the
 1152 Chukchi Borderland, Arctic Ocean. *Quaternary Research*, 63(2), 150–160.
 1153 <https://doi.org/10.1016/j.yqres.2004.12.004>
- 1154 Jakobsson, M., Polyak, L., Edwards, M., Kleman, J., & Coakley, B. J. (2008). Glacial
 1155 geomorphology of the Central Arctic Ocean: the Chukchi Borderland and the Lomonosov
 1156 Ridge. *Earth Surface Processes and Landforms*, 33(4), 526–545.
 1157 <https://doi.org/10.1002/esp.1667>

- 1158 Jakobsson, M., Nilsson, J., O'Regan, M., Backman, J., Löwemark, L., Dowdeswell, J. A., et al.
 1159 (2010). An Arctic Ocean ice shelf during MIS 6 constrained by new geophysical and
 1160 geological data. *Quaternary Science Reviews*, 29(25), 3505–3517.
 1161 <https://doi.org/10.1016/j.quascirev.2010.03.015>
- 1162 Jakobsson, M., Andreassen, K., Bjarnadóttir, L. R., Dove, D., Dowdeswell, J. A., England, J. H.,
 1163 et al. (2014). Arctic Ocean glacial history. *Quaternary Science Reviews*, 92, 40–67.
 1164 <http://dx.doi.org/10.1016/j.quascirev.2013.07.033>
- 1165 Jakobsson, M., Nilsson, J., Anderson, L., Backman, J., Björk, G., Cronin, T. M., et al. (2016).
 1166 Evidence for an ice shelf covering the central Arctic Ocean during the penultimate
 1167 glaciation. *Nature Communications*, 7.
- 1168 Jakobsson, M., Mayer, L. A., Bringensparr, C., Castro, C. F., Mohammad, R., Johnson, P., et al.
 1169 (2020). The International Bathymetric Chart of the Arctic Ocean Version 4.0. *Scientific*
 1170 *Data*, (1), 176.
- 1171 Joe, Y. J., Polyak, L., Schreck, M., Niessen, F., Yoon, S. H., Kong, G. S., & Nam, S.-I. (2020).
 1172 Late Quaternary depositional and glacial history of the Arliss Plateau off the East
 1173 Siberian margin in the western Arctic Ocean. *Quaternary Science Reviews*, 228, 106099.
 1174 <https://doi.org/10.1016/j.quascirev.2019.106099>
- 1175 Jokat, W. (2009). *The Expedition of the Research Vessel “Polarstern” to the Arctic in 2008*
 1176 (ARK-XXIII/3). Alfred Wegener Institute.
- 1177 Kim, J.-H., Hachikubo, A., Kida, M., Minami, H., Lee, D.-H., Jin, Y. K., et al. (2020).
 1178 Upwarding gas source and postgenetic processes in the shallow sediments from the
 1179 ARAON Mounds, Chukchi Sea. *Journal of Natural Gas Science and Engineering*, 76,
 1180 103223.
- 1181 Kirkbride, M. P. (2002). 6 - Processes of glacial transportation. In J. Menzies (Ed.), *Modern and*
 1182 *Past Glacial Environments* (pp. 147–169). Oxford: Butterworth-Heinemann.
 1183 <https://doi.org/10.1016/B978-075064226-2/50009-X>
- 1184 Klages, J. P., Kuhn, G., Graham, A. G. C., Hillenbrand, C.-D., Smith, J. A., Nitsche, F. O., et al.
 1185 (2015). Palaeo-ice stream pathways and retreat style in the easternmost Amundsen Sea
 1186 Embayment, West Antarctica, revealed by combined multibeam bathymetric and seismic
 1187 data. *Geomorphology*, 245, 207–222.
- 1188 Laberg, J. S., Vorren, T. O., Dowdeswell, J. A., Kenyon, N. H., & Taylor, J. (2000). The Andøya
 1189 Slide and the Andøya Canyon, north-eastern Norwegian–Greenland Sea. *Marine*
 1190 *Geology*, 162(2–4), 259–275. [http://dx.doi.org/10.1016/S0025-3227\(99\)00087-0](http://dx.doi.org/10.1016/S0025-3227(99)00087-0)
- 1191 Lisiecki, L. E., & Raymo, M. E. (2005). A Pliocene-Pleistocene stack of 57 globally distributed
 1192 benthic $\delta^{18}O$ records. *Paleoceanography*, 20(1).
- 1193 Lowe, A. L., & Anderson, J. B. (2002). Reconstruction of the West Antarctic ice sheet in Pine
 1194 Island Bay during the Last Glacial Maximum and its subsequent retreat history.
 1195 *Quaternary Science Reviews*, 21(16–17), 1879–1897. [http://dx.doi.org/10.1016/S0277-](http://dx.doi.org/10.1016/S0277-3791(02)00006-9)
 1196 [3791\(02\)00006-9](http://dx.doi.org/10.1016/S0277-3791(02)00006-9)
- 1197 Lowe, A. L., & Anderson, J. B. (2003). Evidence for abundant subglacial meltwater beneath the
 1198 paleo-ice sheet in Pine Island Bay, Antarctica. *Journal of Glaciology*, 49(164), 125–138.

- 1199 MacGregor, J. A., Fahnestock, M. A., Catania, G. A., Aschwanden, A., Clow, G. D., Colgan, W.
 1200 T., et al. (2016). A synthesis of the basal thermal state of the Greenland Ice Sheet.
 1201 *Journal of Geophysical Research: Earth Surface*, 121(7), 1328–1350.
 1202 <https://doi.org/10.1002/2015JF003803>
- 1203 Matthiessen, J., Niessen, F., Stein, R., & Naafs, B. D. A. (2010). Pleistocene glacial marine
 1204 sedimentary environments at the eastern Mendeleev Ridge, Arctic Ocean.
 1205 *Polarforschung*, 79(2), 123–137.
- 1206 Menzies, J., & van der Meer, J. J. M. (2018). *Past Glacial Environments*. (J. Menzies & J. J. M.
 1207 van der Meer, Eds.) (Second). Elsevier.
- 1208 Menzies, J., & Shilts, B. W. (2002). 8 - Subglacial environments. In J. Menzies (Ed.), *Modern
 1209 and Past Glacial Environments* (pp. 183–278). Oxford: Butterworth-Heinemann.
 1210 <https://doi.org/10.1016/B978-075064226-2/50011-8>
- 1211 Miramontes, E., Cattaneo, A., Jouet, G., Th ereau, E., Thomas, Y., Rovere, M., et al. (2016). The
 1212 Pianosa Contourite Depositional System (Northern Tyrrhenian Sea): Drift morphology
 1213 and Plio-Quaternary stratigraphic evolution. *Marine Geology*, 378, 20–42.
 1214 <https://doi.org/10.1016/j.margeo.2015.11.004>
- 1215 Moore, D. G. (1964). Shear strength and related properties of sediments from experimental
 1216 mohole (Guadalupe site). *Journal of Geophysical Research (1896-1977)*, 69(20), 4271–
 1217 4291.
- 1218 Niessen, F., Hong, J. K., Hegewald, A., Matthiessen, J., Stein, R., Kim, H., et al. (2013).
 1219 Repeated Pleistocene glaciation of the East Siberian continental margin. *Nature Geosci*,
 1220 6(10), 842–846. <http://dx.doi.org/10.1038/ngeo1904>
- 1221 Noormets, R., Dowdeswell, J. A., Larter, R. D., Cofaigh, C.  ., & Evans, J. (2009). Morphology
 1222 of the upper continental slope in the Bellingshausen and Amundsen Seas – Implications
 1223 for sedimentary processes at the shelf edge of West Antarctica. *Marine Geology*, 258(1),
 1224 100–114. <https://doi.org/10.1016/j.margeo.2008.11.011>
- 1225   Cofaigh, C., Taylor, J., Dowdeswell, J. A., & Pudsey, C. J. (2003). Palaeo-ice streams, trough
 1226 mouth fans and high-latitude continental slope sedimentation. *Boreas*, 32(1), 37–55.
- 1227   Cofaigh, C., Dowdeswell, J. A., Evans, J., Kenyon, N. H., Taylor, J., Mienert, J., & Wilken,
 1228 M. (2004). Timing and significance of glacially influenced mass-wasting in the
 1229 submarine channels of the Greenland Basin. *Marine Geology*, 207(1), 39–54.
 1230 <https://doi.org/10.1016/j.margeo.2004.02.009>
- 1231   Cofaigh, C., Dowdeswell, J. A., Allen, C. S., Hiemstra, J. F., Pudsey, C. J., Evans, J., &
 1232 Evans, D. [J A. (2005). Flow dynamics and till genesis associated with a marine-based
 1233 Antarctic palaeo-ice stream. *Quaternary Science Reviews*, 24(5), 709–740.
 1234 <https://doi.org/10.1016/j.quascirev.2004.10.006>
- 1235   Cofaigh, C., Hogan, K. A., Dowdeswell, J. A., & Streuff, K. (2016). Stratified glacimarine
 1236 basin-fills in West Greenland fjords. In J. A. Dowdeswell, M. Canals, M. Jakobsson, B. J.
 1237 Todd, E. K. Dowdeswell, & K. A. Hogan (Eds.), *Atlas of Submarine Glacial Landforms:
 1238 Modern, Quaternary and Ancient* (Vol. 46, pp. 99–100). Geological Society, London,
 1239 *Memoirs*.

- 1240 Ó Cofaigh, C., Hogan, K. A., Jennings, A. E., Callard, S. L., Dowdeswell, J. A., Noormets, R., &
 1241 Evans, J. (2018). The role of meltwater in high-latitude trough-mouth fan development:
 1242 The Disko Trough-Mouth Fan, West Greenland. *Marine Geology*, *402*, 17–32.
 1243 <https://doi.org/10.1016/j.margeo.2018.02.001>
- 1244 O’Grady, D. B., & Syvitski, J. P. (2002). Large-scale morphology of Arctic continental slopes:
 1245 the influence of sediment delivery on slope form. In Julian A Dowdeswell & C. Ó
 1246 Cofaigh (Eds.), *SPECIAL PUBLICATION-GEOLOGICAL SOCIETY OF LONDON* (Vol.
 1247 203, pp. 11–32). The Geological Society of London.
- 1248 O’Regan, M., Backman, J., Barrientos, N., Cronin, T. M., Gemery, L., Kirchner, N., et al.
 1249 (2017). The De Long Trough: a newly discovered glacial trough on the East Siberian
 1250 continental margin. *Climate of the Past*, *13*(9), 1269–1284. [https://doi.org/10.5194/cp-13-](https://doi.org/10.5194/cp-13-1269-2017)
 1251 [1269-2017](https://doi.org/10.5194/cp-13-1269-2017)
- 1252 Ottesen, D., & Dowdeswell, J. A. (2006). Assemblages of submarine landforms produced by
 1253 tidewater glaciers in Svalbard. *Journal of Geophysical Research: Earth Surface*, *111*(F1).
 1254 Retrieved from <https://agupubs.onlinelibrary.wiley.com/doi/abs/10.1029/2005JF000330>
- 1255 Ottesen, D., & Dowdeswell, J. A. (2009). An inter-ice-stream glaciated margin: Submarine
 1256 landforms and a geomorphic model based on marine-geophysical data from Svalbard.
 1257 *Geological Society of America Bulletin*, *121*(11–12), 1647–1665.
- 1258 Ottesen, D., Rise, L., Knies, J., Olsen, L., & Henriksen, S. (2005). The Vestfjorden-Trænadjupet
 1259 palaeo-ice stream drainage system, mid-Norwegian continental shelf. *Marine Geology*,
 1260 *218*(1), 175–189. <https://doi.org/10.1016/j.margeo.2005.03.001>
- 1261 Piper, D. J. W., & Normark, W. R. (2009). Processes That Initiate Turbidity Currents and Their
 1262 Influence on Turbidites: A Marine Geology Perspective. *Journal of Sedimentary*
 1263 *Research*, *79*(6), 347–362. <https://doi.org/10.2110/jsr.2009.046>
- 1264 Piper, D. J. W., Deptuck, M., Mosher, D., Hughes Clarke, J., & Migeon, S. (2012). *Erosional*
 1265 *and depositional features of glacial meltwater discharges on the eastern Canadian*
 1266 *continental margin*. (B. Prather, M. E. Deptuck, D. Mohrig, B. van Hoorn, & R. Wynn,
 1267 Eds.), *Applications of the Principles of Seismic Geomorphology to Continental Slope and*
 1268 *Base-of-slope Systems: Case Studies from Seafloor and Near-Seafloor Analogues*. Edited
 1269 by BE Prather, ME Deptuck, D. Mohrig, B. van Hoorn, and R. Wynn. *Society for*
 1270 *Sedimentary Geology (SEPM), Special Publications* (Vol. 99, p. 80). SEPM.
- 1271 Polyak, L., Forman, S. L., Herlihy, F. A., Ivanov, G., & Krinitsky, P. (1997). Late Weichselian
 1272 deglacial history of the Svyataya (Saint) Anna Trough, northern Kara Sea, Arctic Russia.
 1273 *Marine Geology*, *143*(1), 169–188. [https://doi.org/10.1016/S0025-3227\(97\)00096-0](https://doi.org/10.1016/S0025-3227(97)00096-0)
- 1274 Polyak, L., Edwards, M. H., Coakley, B. J., & Jakobsson, M. (2001). Ice shelves in the
 1275 Pleistocene Arctic Ocean inferred from glaciogenic deep-sea bedforms. *Nature*, *410*,
 1276 453–457.
- 1277 Polyak, L., Darby, D. A., Bischof, J. F., & Jakobsson, M. (2007). Stratigraphic constraints on
 1278 late Pleistocene glacial erosion and deglaciation of the Chukchi margin, Arctic Ocean.
 1279 *Quaternary Research*, *67*(2), 234–245. <https://doi.org/10.1016/j.yqres.2006.08.001>

- 1280 Polyak, L., Best, K. M., Crawford, K. A., Council, E. A., & St-Onge, G. (2013). Quaternary
 1281 history of sea ice in the western Arctic Ocean based on foraminifera. *Quaternary Science*
 1282 *Reviews*, 79, 145–156. <https://doi.org/10.1016/j.quascirev.2012.12.018>
- 1283 Pope, E. L., Talling, P. J., & Ó Cofaigh, C. (2018). The relationship between ice sheets and
 1284 submarine mass movements in the Nordic Seas during the Quaternary. *Earth-Science*
 1285 *Reviews*, 178, 208–256. <https://doi.org/10.1016/j.earscirev.2018.01.007>
- 1286 Rebesco, M., & Camerlenghi, A. (2008). Late Pliocene margin development and mega debris
 1287 flow deposits on the Antarctic continental margins: Evidence of the onset of the modern
 1288 Antarctic Ice Sheet? *Palaeogeography, Palaeoclimatology, Palaeoecology*, 260(1), 149–
 1289 167. <https://doi.org/10.1016/j.palaeo.2007.08.009>
- 1290 Rebesco, M., Özmaral, A., Urgeles, R., Accettella, D., Lucchi, R. G., Rütther, D., et al. (2016).
 1291 Evolution of a high-latitude sediment drift inside a glacially-carved trough based on high-
 1292 resolution seismic stratigraphy (Kveithola, NW Barents Sea). *Quaternary Science*
 1293 *Reviews*, 147(Special Issue: PAST Gateways (Palaeo-Arctic Spatial and Temporal
 1294 Gateways)), 178–193. <http://dx.doi.org/10.1016/j.quascirev.2016.02.007>
- 1295 Rydningen, T. A., Laberg, J. S., & Kolstad, V. (2015). Seabed morphology and sedimentary
 1296 processes on high-gradient trough mouth fans offshore Troms, northern Norway.
 1297 *Geomorphology*, 246, 205–219. <http://dx.doi.org/10.1016/j.geomorph.2015.06.007>
- 1298 Schomacker, A., Kjær, K. H., & Krüger, J. (2010). 8 Subglacial Environments, Sediments and
 1299 Landforms at the Margins of Mýrdalsjökull. In A. Schomacker, J. Krüger, & K. H. Kjær
 1300 (Eds.), *The Mýrdalsjökull Ice Cap, Iceland. Glacial processes, sediments and landforms*
 1301 *on an active volcano* (Vol. 13, pp. 127–144). Elsevier. [https://doi.org/10.1016/S1571-](https://doi.org/10.1016/S1571-0866(09)01308-6)
 1302 0866(09)01308-6
- 1303 Schreck, M., Nam, S.-I., Polyak, L., Vogt, C., Kong, G.-S., Stein, R., et al. (2018). Improved
 1304 Pleistocene sediment stratigraphy and paleoenvironmental implications for the western
 1305 Arctic Ocean off the East Siberian and Chukchi margins. *Arktos*, 4(1), 21.
 1306 <https://doi.org/10.1007/s41063-018-0057-8>
- 1307 Shaver, R., & Hunkins, K. (1964). Arctic ocean geophysical studies: Chukchi Cap and Chukchi
 1308 abyssal plain. *Deep Sea Research and Oceanographic Abstracts*, 11(6), 905–916.
 1309 [https://doi.org/10.1016/0011-7471\(64\)90340-7](https://doi.org/10.1016/0011-7471(64)90340-7)
- 1310 Shipp, S. S., Anderson, J., & Domack, E. (1999). Late Pleistocene–Holocene retreat of the West
 1311 Antarctic Ice-Sheet system in the Ross Sea: part 1—geophysical results. *Geological*
 1312 *Society of America Bulletin*, 111(10), 1486–1516.
- 1313 Solheim, A., Faleide, J. I., Andersen, E. S., Elverhøi, A., Forsberg, C. F., Vanneste, K., et al.
 1314 (1998). Late Cenozoic Seismic Stratigraphy And Glacial Geological Development Of
 1315 The East Greenland And Svalbard--Barents Sea Continental Margins. *Quaternary*
 1316 *Science Reviews*, 17(1), 155–184. [https://doi.org/10.1016/S0277-3791\(97\)00068-1](https://doi.org/10.1016/S0277-3791(97)00068-1)
- 1317 Stein, R., Matthießen, J., Niessen, F., Krylov, A., Nam, S., & Bazhenova, E. (2010). Towards a
 1318 better (litho-) stratigraphy and reconstruction of Quaternary paleoenvironment in the
 1319 Amerasian Basin (Arctic Ocean). *Polarforschung*, 79(2), 97–121.

- 1320 Stewart, M. A., & Lonergan, L. (2011). Seven glacial cycles in the middle-late Pleistocene of
 1321 northwest Europe: Geomorphic evidence from buried tunnel valleys. *Geology*, 39(3),
 1322 283–286. <https://doi.org/10.1130/G31631.1>
- 1323 SWERUS Scientific Party. (2016). *Cruise Report SWERUS-C3 Leg 2*.
- 1324 Taylor, J., Dowdeswell, J. A., Kenyon, N. H., & Ó Cofaigh, C. (2002). Late Quaternary
 1325 architecture of trough-mouth fans: debris flows and suspended sediments on the
 1326 Norwegian margin. In Julian A Dowdeswell & C. Ó Cofaigh (Eds.), *Glacier-influenced*
 1327 *sedimentation on high-latitude continental margins* (pp. 55–71). The Geological Society
 1328 of London. <https://doi.org/10.1144/GSL.SP.2002.203.01.04>
- 1329 Todd, B. J., Valentine, P. C., Longva, O., & Shaw, J. (2007). Glacial landforms on German
 1330 Bank, Scotian Shelf: evidence for Late Wisconsinan ice-sheet dynamics and implications
 1331 for the formation of De Geer moraines. *Boreas*, 36(2), 148–169.
 1332 <https://doi.org/10.1111/j.1502-3885.2007.tb01189.x>
- 1333 Veeken, P. C. H., & van Moerkerken, B. (2013). *Seismic Stratigraphy and Depositional Facies*
 1334 *Models*. EAGE publications.
- 1335 Vorren, T. O., & Laberg, J. S. (1997). Trough mouth fans—palaeoclimate and ice-sheet
 1336 monitors. *Quaternary Science Reviews*, 16(8), 865–881.
- 1337 Wang, R., Xiao, W., März, C., & Li, Q. (2013). Late Quaternary paleoenvironmental changes
 1338 revealed by multi-proxy records from the Chukchi Abyssal Plain, western Arctic Ocean.
 1339 *Global and Planetary Change*, 108, 100–118.
 1340 <https://doi.org/10.1016/j.gloplacha.2013.05.017>
- 1341 Wellner, J. S., Lowe, A. L., Shipp, S. S., & Anderson, J. B. (2001). Distribution of glacial
 1342 geomorphic features on the Antarctic continental shelf and correlation with substrate:
 1343 implications for ice behavior. *Journal of Glaciology*, 47(158), 397–411.
 1344 <https://doi.org/10.3189/172756501781832043>
- 1345 Wellner, J. S., Heroy, D. C., & Anderson, J. B. (2006). The death mask of the antarctic ice sheet:
 1346 Comparison of glacial geomorphic features across the continental shelf. *Geomorphology*,
 1347 75(1), 157–171. <https://doi.org/10.1016/j.geomorph.2005.05.015>
- 1348 Wille, P. (2005). *Sound images of the ocean: in research and monitoring* (Vol. 1). Springer
 1349 Science & Business Media.
- 1350 Winsborrow, M. C. M., Clark, C. D., & Stokes, C. R. (2010). What controls the location of ice
 1351 streams? *Earth-Science Reviews*, 103(1–2), 45–59.
 1352 <http://dx.doi.org/10.1016/j.earscirev.2010.07.003>
- 1353 Zaragosi, S., Auffret, G. A., Faugères, J.-C., Garlan, T., Pujol, C., & Cortijo, E. (2000).
 1354 Physiography and recent sediment distribution of the Celtic Deep-Sea Fan, Bay of
 1355 Biscay. *Marine Geology*, 169(1), 207–237.

1356

1357

1358